

A new role for PHYHD1 and related dioxygenases: demethylation of 2'-O-methylated nucleosides

Justas Stonkus ^{1,*}, Rasa Rutkienė ¹, Rita Meškienė ¹, Martyna Jasiūnienė ¹,
Agota Aučynaitė ¹, Laura Kalinienė ¹, Justas Lazutka ², Darius Balčiūnas ^{2,3},
Giedrius Vilkaitis ², Rolandas Meškys ¹

¹Institute of Biochemistry, Life Sciences Center, Vilnius University, Vilnius LT-10257, Lithuania

²Institute of Biotechnology, Life Sciences Center, Vilnius University, Vilnius LT-10257, Lithuania

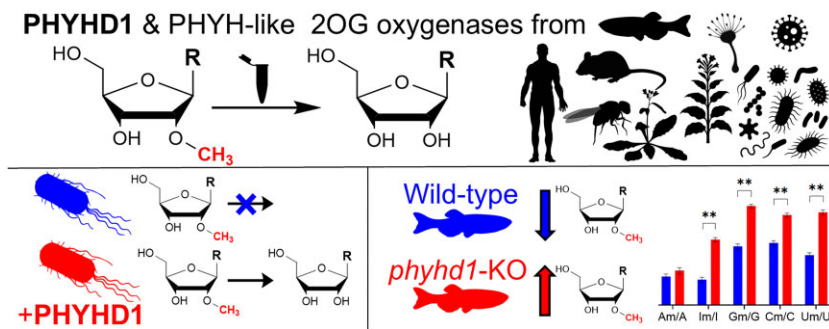
³Department of Biology, Temple University, Philadelphia, PA 19122, United States

*To whom correspondence should be addressed. Email: justas.stonkus@gmc.stud.vu.lt

Abstract

Nucleoside 2'-O-methylation is a widespread RNA modification found across diverse RNA types in all domains of life. Although considerable progress has been made in mapping 2'-O-methylation sites and elucidating their biological roles, the enzymatic pathways responsible for the catabolism of 2'-O-methylated nucleosides remain largely unexplored. Here, we report a previously unidentified 2'-O-methylated nucleoside demethylation reaction catalyzed by a metagenome-derived bacterial dioxygenase named FJS. We further show that FJS-related enzymes, including human phytanoyl-CoA dioxygenase domain-containing protein 1 (PHYHD1), catalyze the 2-oxoglutarate-dependent demethylation of a broad range of ribose-methylated nucleosides, but do not act on modified nucleotides or 3'-terminal 2'-O-methylated RNA substrates. To determine whether the loss of PHYHD1 function affects 2'-O-methylation levels of RNA-incorporated or free nucleosides, we generated a *phyhd1* knockout zebrafish line. While RNA modification levels remained unchanged, the amount of free 2'-O-methylated nucleosides was significantly elevated in both *phyhd1* knockout embryos and adult zebrafish. These findings indicate that PHYHD1 does not directly demethylate RNA but instead functions in the turnover of free 2'-O-methylated nucleosides. Together, our study identifies a previously unrecognized metabolic pathway for 2'-O-methylated nucleosides and defines PHYHD1 as the key dioxygenase involved in their demethylation, providing new insights into the catabolism of modified nucleosides.

Graphical abstract



Introduction

RNA modifications play a crucial role in RNA folding, stability, and RNA–protein interactions, making them essential for RNA function and gene expression regulation [1]. Among these modifications, 2'-O-methylation (2'-O-Me, Nm) is one of the most abundant, found across all major RNA classes within all domains of life [2]. It is well established that these modifications increase RNA resistance and frequently support interactions with auxiliary proteins [2]. Extensive research has explored 2'-O-Me across diverse RNA types, including tRNA, rRNA, the 5' cap of mRNA, long non-coding and small non-coding RNAs, such as small nuclear RNA (snRNA), mi-

croRNA (miRNA), and PIWI-interacting RNA (piRNA), as well as its potential links to different diseases [2, 3]. Recent advances in detection sensitivity [4] have greatly improved our understanding of the distribution [5] and functions [6] of internal (non-cap) mRNA 2'-O-Me groups, as well as the dynamic regulation of rRNA and tRNA 2'-O-methylation during development in model organisms such as zebrafish [7] and mice [8].

Beyond its biological significance, 2'-O-methylation is widely used in biotechnology and medicine. It enhances the stability of aptamers [9], advances the efficiency and precision of CRISPR (clustered regularly interspaced palindromic

Received: June 7, 2025. Revised: November 12, 2025. Accepted: November 13, 2025

© The Author(s) 2025. Published by Oxford University Press.

This is an Open Access article distributed under the terms of the Creative Commons Attribution License (<https://creativecommons.org/licenses/by/4.0/>), which permits unrestricted reuse, distribution, and reproduction in any medium, provided the original work is properly cited.

repeats) RNA-based gene editing [10, 11], and plays a key role in developing therapeutic oligonucleotides, such as small interfering RNAs [12]. The addition of 2'-O-Me groups improves the pharmacokinetics of RNA-based treatments by reducing immunogenicity, extending half-life, and increasing binding affinity [12]. Therefore, understanding the effects of 2'-O-methylation on cellular function and the mechanisms governing the metabolism of these modified nucleotides remains a critical area of research with broad implications for both basic biology and therapeutic innovation.

While the exact mechanisms by which 2'-O-Me groups influence cellular functions are known only for a subset of RNA sites [13], it is well established that 2'-O-methylation enhances RNA stability by protecting against chemical and enzymatic hydrolysis [14]. One well-characterized example is the 3'-end 2'-O-methylation of small RNAs catalyzed by Hen1, which prevents 3'-5' exonucleolytic degradation and 3'-uridylation [15]. Increased stability is also observed in RNA molecules carrying internal 2'-O-methyl groups, such as methylated mRNA [16]. Beyond their stabilizing role, 2'-O-Me groups influence RNA secondary structure by shifting the ribose conformation toward the C3'-endo form [17], a structural feature essential for the proper function of rRNA and tRNA [13]. Accordingly, many 2'-O-methylation sites are site specific and guided by C/D box small nucleolar RNAs (snoRNAs; primarily in rRNA [2]), small Cajal body-specific RNAs (scaRNAs; in snRNA [18]), or dedicated stand-alone enzymes such as yeast tRNA methyltransferases [19]. However, it remains unclear whether non-cap mRNA riboses are methylated by small nucleolar ribonucleoproteins (snoRNPs), stand-alone enzymes, or both [2].

Although some knowledge exists on how RNA-guided enzyme complexes and single-acting enzymes introduce 2'-O-Me groups post-transcriptionally, there are very few data on the catabolism, salvage pathways, or potential *in situ* demethylation of 2'-O-methylated nucleosides and nucleotides. Only a few studies have characterized enzymes involved in the biodegradation of 2'-O-methylated nucleosides. The first reported enzyme with activity toward 2'-O-methylribonucleosides is *LbNH*, a nucleoside hydrolase from *Lactobacillus buchneri* [20]. *LbNH* hydrolyses 2'-O-methylated nucleosides, producing 2'-O-methylribose and the corresponding nucleobase. Additionally, though with low efficiency, it can catalyze a transribosylation reaction between 2'-O-Me nucleosides and nucleobases [21]. A similar hydrolase, *AgNH*, purified from *Agromyces* sp. MM-1 cells [22], catalyzes this transribosylation reaction with a slightly higher yield. Another noteworthy enzyme is *RK9NH*, identified from a soil-based metagenomic library. In addition to hydrolysing natural substrates such as 2'-O-methyluridine, hydrolase *RK9NH* efficiently processes fluorinated analogues, including 5-fluorouridine, 5-fluoro-2'-deoxyuridine, and 5-fluoro-2'-O-methyluridine, into 5-fluorouracil [23]. The *RK9NH* gene was identified alongside a gene encoding an aldolase, homologous to 2-deoxy-D-ribose 5-phosphate aldolase (DERA) from *Escherichia coli*, suggesting a potential gene cluster involved in the degradation of 2'-O-methylated nucleosides [23]. However, to date, RNA 2'-O-Me groups have no known erasers, and this modification is considered irreversible [2].

Nevertheless, other nucleoside methyl modifications have known erasers, primarily enzymes from the 2-oxoglutarate-

and Fe(II)-dependent oxygenase superfamily (2OG oxygenases, EC 1.14.11). Notable examples include the AlkB family members FTO [24] and AlkBH5 [25], which function as 2OG/Fe(II)-dependent demethylases targeting the N⁶-methyladenosine (m⁶A) modification in mRNA. In addition to RNA-incorporated substrates, 2OG/Fe(II)-dependent dioxygenases can also act on free nucleosides. One such example is the recently characterized nucleoside 2'-hydroxylase (PDN2'H) from *Neurospora crassa* [26]. Generally, 2OG oxygenases couple the decarboxylation of 2-oxoglutarate to the oxidation of C–H bonds in a wide range of substrates [27]. As a result, they are involved in numerous cellular processes, including the synthesis and catabolism of diverse compounds, oxygen sensing, and the regulation of transcription, translation, and protein stability [27]. Typically, 2OG oxygenase-catalyzed oxidation of the primary substrate yields a hydroxylated product; however, when the target carbon is adjacent to a heteroatom, hydroxylation can lead to demethylation [28].

This study describes a novel enzymatic activity within the 2OG oxygenase superfamily, specifically in enzymes belonging to or closely related to the phytanoyl-CoA dioxygenase domain-containing 1 (PHYHD1) protein group. The domain name originates from phytanoyl-CoA dioxygenase (PHYH, also known as PAHX). Human PHYH is a peroxisomal enzyme that catalyzes the breakdown of phytanic acid, which cannot undergo β-oxidation due to its 3-methyl group [29]. The closest homolog of PHYH is the aforementioned PHYHD1, which is present in both the nucleus and the cytoplasm [30]. Human PHYHD1 (hPHYHD1) exists in three isoforms (A, B, and C), with isoform A catalysing the iron-dependent conversion of 2-oxoglutarate to succinate and CO₂ *in vitro* [31]. In addition, hPHYHD1 binds mRNA and interacts with proteins involved in cell division and mRNA splicing in HEK293T cells [30]. It has also been implicated in various carcinomas [32, 33], pituitary adenomas [34], and neurodegenerative diseases, especially Alzheimer's disease [35–37].

Homologs of human PHYHD1 are broadly conserved across animals and have been studied in several species. For instance, knockout of the PHYHD1 gene in silkworms results in increased egg size [38], while its up-regulation in immune cells has been associated with physiological abnormalities in *Xenopus* tadpoles [39] and T-cell stimulation in mice [40]. Moreover, databases such as GenBank [41] contain many microbial dioxygenase sequences annotated as phytanoyl-CoA dioxygenase family proteins, referred to here as PHYH-like proteins.

Despite extensive investigation, no physiological substrate had previously been identified for hPHYHD1 [30, 31]. Here, we demonstrate that both eukaryotic and prokaryotic PHYHD1 and PHYH-like enzymes catalyze the oxidative demethylation of 2'-O-methylated nucleosides, suggesting a conserved role in the catabolism of these modified metabolites. Notably, we show that PHYHD1 does not demethylate phosphorylated nucleosides or RNA *in vitro*. Furthermore, we demonstrate that loss of PHYHD1 function in zebrafish does not alter total RNA or mRNA 2'-O-Me levels. Instead, zebrafish PHYHD1 knockouts display a significant accumulation of free 2'-O-methylated nucleosides. Together with genome-wide association data and previous biochemical evidence, our findings indicate that non-incorporated (free) 2'-O-methyl nucleosides serve as the primary physiological substrate of PHYHD1.

Materials and methods

Reagents

If not stated otherwise, 2'-O-methyl nucleosides and 2'-O-methyl nucleoside triphosphates were purchased from Jena Bioscience (Germany). N⁶,2'-O-dimethyladenosine, N⁴,2'-O-dimethylcytidine, N⁴-acetyl-2'-O-methylcytidine, and N⁴-benzoyl-2'-O-methylcytidine were purchased from BLD Pharm (China); N⁶-methyladenosine was purchased from Aaron Chemicals (USA); and N⁴-acetylcytidine was purchased from Combi-Blocks (USA). Other nucleosides used for standards were purchased from Sigma-Aldrich (Germany). Reagents and solvents were purchased from VWR International (Austria) and Honeywell (Germany). Enzymes and other reagents for standard microbiology and molecular biology procedures were obtained from Thermo Fisher Scientific (Lithuania) and Carl Roth (Germany). The plasmid purification kit (ZR Plasmid Miniprep-Classic, #D4054) was purchased from Zymo Research (USA).

Biological resources

Escherichia coli DH5 α (Pharmacia, USA) was used for routine DNA manipulations. The *E. coli* HMS174 (DE3) (Novagen, USA) and *E. coli* LOBSTR (DE3) [42] strains were used for recombinant protein synthesis. The construction of the *E. coli* DH10B Δ pyrFEC strain was described previously [43], and the HMS174(DE3) Δ pyrF strain was constructed using the same methodology. The wild-type zebrafish (*Danio rerio*) AB line was obtained from the European Zebrafish Resource Center (EZRC).

Metagenomic library construction and screening

The methods for constructing and screening soil-based metagenomic libraries were described previously [23, 43, 44]. Briefly, we used a uridine/cytidine auxotrophic *E. coli* DH10B strain, in which three *pyr* operon genes (*pyrF*, *pyrE*, and *pyrC*) required for *de novo* pyrimidine synthesis had been disrupted (*E. coli* DH10B Δ pyrF Δ pyrE Δ pyrC::Km, referred to as *E. coli* DH10B Δ pyrFEC in this study). To select genes involved in 2'-O-methylcytidine biodegradation, the *E. coli* DH10B Δ pyrFEC strain was transformed with soil-derived metagenomic libraries and grown on M9 medium supplemented with 10 mg/l 2'-O-methylcytidine. The sequence of the isolated metagenomic plasmid was identified using Nanopore sequencing (SeqVision, Lithuania).

Plasmid construction

Plasmids used in this study were constructed using aLICator LIC Cloning and Expression Kit 3 (Thermo Fisher Scientific, Lithuania, #K1291) or synthesized by Twist Bioscience (USA). Detailed plasmid construction procedures are described in the Supplementary Data. The sequences of primers used for molecular cloning are available in [Supplementary Table S1](#).

Recombinant protein biosynthesis and purification

Escherichia coli HMS174 or *E. coli* LOBSTR cells transformed with the required plasmid DNA were grown overnight in LB medium with 100 μ g/ml ampicillin under aerobic conditions at 30°C. Then, 0.05 or 0.2 ml of the overnight culture was transferred into 50 or 200 ml of fresh LB medium supplemented with ampicillin. The cells were then grown aerobically at 30°C to an optical density (OD₆₀₀) of 0.4–0.5; at this

point, protein synthesis was induced with 0.5 mM isopropyl- β -D-thiogalactopyranoside (IPTG). Following induction, cells were incubated at 30°C for 4 h, then centrifuged at >10 000 rcf for 15 min at 4°C to pellet the cells and remove the growth medium.

For the preparation of the cell-free extract, the pellet was resuspended in 5–10 ml of lysis buffer [50 mM Tris-HCl, 300 mM KCl, 10% glycerol, and 1 mM phenylmethylsulfonyl fluoride (PMSF), pH 8.0] and lysed by sonication at 22 kHz in an ice–water bath. Sonication was performed using a Branson SFC250 sonifier with a 13 mm probe at 30% amplitude for 3 min (5 s sonication with 10 s breaks). The lysate was centrifuged at >10 000 rcf for 15 min at 4°C to separate the soluble and insoluble fractions. Protein purification and desalting were performed using an ÄKTA pure 25 M protein purification system (Cytiva, Sweden). The soluble fraction was applied onto a 1 ml HiTrap Chelating HP column (Cytiva, Sweden, #17 524 701) charged with Ni²⁺ ions and equilibrated with buffer A (50 mM Tris-HCl, pH 8.0, 300 mM KCl, 10% glycerol). After washing with at least five column volumes of buffer A, His-tagged proteins were eluted using a linear imidazole gradient (0–0.35 M) in buffer A at a 1 ml/min flow rate. The fractions containing the purified proteins were pooled and loaded onto a HiTrap Desalting column with Sephadex G-25 resin (Cytiva, Sweden, #17 140 801), then eluted with 50 mM Tris-HCl, pH 8.0, supplemented with 10% glycerol. If needed, the purified proteins were concentrated using Amicon Ultra-4 Centrifugal Filter Units with a 10 kDa molecular weight cut-off (MWCO) membrane (Merck Millipore, Ireland, #UFC801024). Protein concentrations were determined using an Implen NanoPhotometer NP80 UV/VIS spectrophotometer, with extinction coefficients calculated based on amino acid composition using the ExPASy ProtParam tool [45].

Demethylase activity screening using *E. coli* HMS174(DE3) Δ pyrF bacterial strain

To assess demethylation activity, *E. coli* HMS174(DE3) Δ pyrF cells were transformed with plasmids carrying genes encoding selected 2OG oxygenases in expression vectors (pET-21 and pLATE31). Transformed cells were first grown on LB agar plates, and a single colony was transferred to 5 ml of liquid LB medium and incubated at 37°C for 4 h. The culture was then diluted to an OD₆₀₀ of 0.5. A 1 ml aliquot of the diluted culture was taken and washed several times with physiological solution, diluted 20-fold, and plated by applying 2 μ l spots onto M9 medium supplemented with either 10 mg/l 2'-O-methylcytidine, 10 mg/l 2'-O-methyluridine, or 10 mg/l uridine (positive control), with a no-substrate medium serving as a negative control.

Enzyme activity assay using TLC and HPLC-MS

Standard reaction mixtures (40 μ l) contained 10 μ l of purified enzyme (10 μ M for quantitative reactions and 2–10 mg/ml for qualitative reactions), 5 mM 2'-O-methylated nucleoside substrate, 10 mM 2-oxoglutarate, 0.5 mM FeSO₄, and 1 mM ascorbate in 50 mM Tris-HCl (pH 8.0) buffer. Thin-layer chromatography (TLC) analyses were performed using Supelco TLC Silica gel 60 F₂₅₄ plates (Merck, Germany, #105 554) with chloroform:methanol mobile phases at a 9:1 v/v or 7:3 v/v ratio. For high-performance liquid chromatography–mass spectrometry (HPLC-MS) analysis, re-

action mixtures were quenched by adding 40 μ l of acetonitrile, vortexed for 1 min, and centrifuged to remove denatured protein. HPLC-MS analyses were performed using an HPLC system (Shimadzu, Japan) equipped with a photodiode array (PDA) detector (Shimadzu, Japan) and a mass spectrometer (LCMS 2020, Shimadzu, Japan). Chromatographic separation was conducted at 40°C using a 150 \times 3 mm YMC-Pack Pro C18 column (YMC, Japan, #AS12S03-1503WT). Data were analysed using LabSolutions software version 5.42 SP6 (Shimadzu, Japan).

Purpald test for formaldehyde detection

The formation of formaldehyde during the demethylation of 2'-O-methylcytidine was determined spectrophotometrically using the Purpald reagent (4-amino-3-hydrazino-5-mercaptop-1,2,4-triazole, Fluka, Switzerland, #08 095). The reaction was initiated by adding the purified enzyme to the standard reaction mixture, excluding FeSO_4 . All assays were incubated at 37°C for 1 h and stopped by adding 250 μ l of 100 mM Purpald solution in 1 M NaOH. After a 10 min incubation at 30°C, absorbance was measured at 550 nm.

2'-O-Methyl nucleoside 5'-monophosphate synthesis

2'-O-Methyl nucleoside 5'-monophosphate synthesis was performed as previously described [46]. Briefly, the 2'-O-methyl nucleoside monophosphorylation reaction was carried out in a 1.5 ml reaction mixture containing 50 mM 2'-O-methyl nucleoside, 5 mM GTP (or 5 mM ATP for 2'-O-methylguanosine monophosphorylation), 7 mM MgCl_2 , 300 mM acetyl phosphate, 0.1 mg/ml *Drosophila melanogaster* deoxynucleoside kinase, and 0.25 mg/ml *E. coli* acetate kinase in 50 mM potassium phosphate buffer (pH 7.5). The reaction was performed at 37°C and 500 rpm for 24 h. The formation of 2'-O-methyl nucleoside 5'-monophosphates was qualitatively detected using TLC and HPLC-MS analyses.

Phylogenetic and sequence analysis of 2OG oxygenases

The sequence alignment for the Supplementary Tree, which includes all reviewed protein sequences with 2-oxoglutarate-dependent dioxygenase activity from the UniProtKB dataset [47], was performed using the MAFFT online service [48]. The tree was constructed using the UPGMA method and visualized with iTOL [49]. For Fig. 2, the sequence alignment and phylogenetic tree of selected FJS homologs were generated using the ClustalW algorithm [50] and the Maximum Likelihood method in MEGA11 [51]. The evolutionary history was inferred using the Maximum Likelihood method and JTT matrix-based model [52]. The tree with the highest log-likelihood (-14185.86) is presented. The percentage of replicate trees in which the associated taxa clustered together in the bootstrap test (1000 replicates) is shown next to the branches [53]. All evolutionary analyses were conducted in MEGA11 [51].

Protein structure analysis and molecular docking

Crystal structures of human PHYHD1 in complex with 2-oxoglutarate and iron (PDB ID: 3OBZ) [31], and human PHYH (PAHX) in complex with 2-oxoglutarate and iron (PDB ID: 2A1X) [29], along with protein structures predicted

using AlphaFold 3 [54], were used for structural comparisons. Molecular docking on the PHYHD1 structure (PDB ID: 3OBZ) was performed using the Attracting Cavities 2.0 [55] algorithm (box centre: -29 - 128 - 66, box size: 17 - 17 - 17, number of random initial conditions: 4, sampling exhaustivity: medium, cavity prioritization: buried) via the Swissdock server [56]. The docking results with the lowest SwissParam values (ΔG_{SP}) are presented. Molecular graphics and structural analyses were conducted using UCSF ChimeraX [57]. Active centre cavity volumes for the human PHYHD1 crystal structure (PDB ID: 3OBZ) and the predicted structure of human PHYH were calculated using the pyKVFinder package [58].

miR173/miR173*^{CH3} duplex demethylation assay using the periodate oxidation method

Demethylation activity was assessed using the periodate oxidation method. The enzymes were incubated with a hemimethylated RNA duplex composed of miR173*^{CH3} strand (21 nt), which was 5'-phosphorylated using [γ -³³P]ATP and contained a 3'-terminal 2'-O-methylguanosine (5'-P³²GAUUCUCUGUGUAAGCGAAA[2'-OmG]-3'), along with a complementary miR173-1 (22 nt) strand (5'-UUCGCUUGCAGAGAGAAUCAC-3'), or 3'-terminal 2'-O-methylcytidine. The reaction mixture (10 μ l total volume) contained 0.1 μ M RNA duplex, 5 or 100 μ M oxygenase, 10 mM 2-oxoglutarate, 1 mM ascorbate, and 0.25 mM FeSO_4 in 50 mM Tris-HCl (pH 8.0). Incubation was carried out at 30°C for 4 h, followed by periodate treatment as previously described [59]. The reaction products were resolved using 15% urea-polyacrylamide gel electrophoresis (PAGE) and visualized via phosphorescence using a FLA-5100 Image Reader (Fujifilm) and MultiGauge V3.0 software.

Zebrafish husbandry

Zebrafish stocks were maintained under standard conditions at 27–27.5°C with a 14:10 h light/dark cycle, a pH value of 7.4, and controlled salinity (Vet. Approval No. LT 59-13-002, LT 61-13-007). All experimental procedures were approved by the Lithuanian State Food and Veterinary Service (approval no. G2-258). F_3 mutant *phyhd1*-knockout (KO) and wild-type (WT) AB zebrafish (starting $n = 60$; $n = 40$ at the time of euthanasia) used for phenotypic and RNA 2'-O-methyl nucleoside level comparisons were raised in the same tank until sexual maturity (3 months). The embryos were transferred to the same tank 5 days post-fertilization (dpf) and then moved to a larger tank at 30 dpf. The WT and *phyhd1*-KO fish were then euthanized using 0.4% (w/v) tricaine (Sigma-Aldrich, Germany, #E10521) solution, measured and weighed, tail-clipped, and stored at -80°C.

Preparation of guide RNA

Guide RNAs (gRNAs) were prepared by combining 3 μ l of 50 μ M Alt-R tracrRNA (Integrated DNA Technologies, USA, #1 072 533) with 3 μ l of custom 50 μ M Alt-R crRNA (Integrated DNA Technologies, USA) and 44 μ l of RNase-free Duplex buffer (Integrated DNA Technologies, USA, #11-01-03-01). The mixture was then incubated in a thermal cycler at 95°C for 5 min, followed by a cool down at 1°C/min for 70 min until the temperature reached 25°C. The resulting 3 μ M gRNAs were aliquoted and stored at -80°C.

mRNA synthesis

The pT3TS-nCas9n plasmid [60] was linearized with *Xba*I and transcribed using the T3 mMessage mMachine *in vitro* transcription kit (Thermo Fisher Scientific, USA, #AM1348). The transcribed mRNA was purified using the RNeasy MinElute kit (Qiagen, Germany, #74 204), diluted to 150 ng/μl (nCas9n) in RNase-free water, and separated into 2 μl portions, which were then stored at -80°C.

Generation of zebrafish *phyhd1*-KO mutant line

CRISPR/CRISPR-associated protein 9 (Cas9) editing was performed using synthesized nCas9n mRNA and two gRNAs (GTCTCTAGTGACTCCTCACC; GGCTGTCTGTG-GTTCATCCC) flanking the PHYHD1 active site-coding region. The two 3 μM gRNAs were mixed in a 1:1 ratio, and 8 μl of the resulting mixture was combined with 2 μl of 150 ng/μl nCas9 mRNA. A 3 nl volume of the nCas9n mRNA/gRNA mix was injected into the yolk of 1-cell stage AB strain zebrafish embryos. F₀ adults capable of transmitting the deletion were selected and outcrossed to generate heterozygous F₁ fish. F₁ adult fish were tail-clipped and genotyped by PCR and DNA sequencing of the extracted PCR bands (genotyping primer sequences available in *Supplementary Table S1*). Positive mutants were incrossed to produce homozygous F₂ fish (*n* = 5; 3 female, 2 male). F₃ embryos and adult fish were used for subsequent studies.

Zebrafish total and messenger RNA extraction

Total RNA from zebrafish embryos [24 h post-fertilization (hpf)] and adults (3 months post-fertilization) was extracted using TRI Reagent (Zymo Research, USA, #R2050-1-200) and Direct-zol RNA Miniprep Plus (Zymo Research, USA, #R2072) with an additional DNase I digestion step. Each sample consisted of either a single adult fish or 10 embryos. Zebrafish embryo (24 hpf) and adult (3 months post-fertilization) mRNA was directly purified from cell lysate using the Dynabeads mRNA DIRECT Purification Kit (Thermo Fisher Scientific, Lithuania, #61 011), with an additional rRNA contamination elimination step. Each sample consisted of 30 embryos or a single adult zebrafish. The quality of purified mRNA was assessed by capillary electrophoresis using an RNA 6000 Pico Kit on a Bioanalyzer 2100 (Agilent Technologies, USA, #NC1711873).

RNA hydrolysis

Purified mRNA was first incubated with RNA 5' pyrophosphohydrolase (RppH, New England Biolabs, USA, #M0356S) in NEB buffer 2 according to the manufacturer's instructions. Total RNA and decapped mRNA were first heat-denatured for 5 min at 95°C and then subjected to digestion at 37°C for 16 h using 250 U of Pierce Universal Nuclease for Cell Lysis (Thermo Fisher Scientific, Lithuania, #88 702), 0.005 U of phosphodiesterase I from *Crotalus adamanteus* venom (Sigma-Aldrich, USA, #P3243), and 2 U of FastAP Thermosensitive Alkaline Phosphatase (Thermo Fisher Scientific, Lithuania, #EF0654). After incubation, one volume of acetonitrile was added. The resulting mixture was incubated at 37°C for 10 min and then centrifuged to remove denatured protein.

Extraction and quantification of free nucleosides from zebrafish embryos and adults

Zebrafish embryos (24 hpf; *n* = 50) were resuspended in 200 μl of TE buffer (10 mM Tris-HCl, 1 mM EDTA, pH 8.0), heated at 95°C for 5 min, and digested by adding 20 μl of Proteinase K (Thermo Fisher Scientific, Lithuania, #EO0492). The mixture was incubated at 55°C for 1 h, with gentle mixing by pipetting every 20 min. Subsequently, two volumes of ice-cold acetonitrile (440 μl) were added, and the samples were incubated at -20°C for 1 h. Then, the soluble and insoluble fractions were separated by centrifugation at >30 000 rpm for 15 min at 4°C, and the resulting supernatant was centrifuged again to remove remaining debris.

Nucleosides from frozen (-80°C) adult zebrafish (euthanized with tricaine 3 months post-fertilization) were extracted using the same procedure with double the reagent volumes. The nucleoside-containing extracts were concentrated under vacuum using a Savant Automatic Environmental SpeedVac System AES1010 to ~30 μl (for embryos) or 100 μl (for adults), and then centrifuged to separate the acetonitrile and lipid phases. The upper phase was analysed using HPLC-tandem MS (HPLC-MS/MS) as described below.

Detection and quantification of nm/N ratios

Hydrolysed RNA supernatants and free nucleoside extracts were analysed by HPLC-MS/MS using a Nexera X2 UHPLC system coupled to an LCMS-8050 mass spectrometer (Shimadzu, Japan) equipped with an electrospray ionization (ESI) source. Chromatographic separation was performed on a 3 × 150 mm YMC-Triart C18 column (particle size 3 μm; YMC, Japan, #TA12S03-1503WT) maintained at 40°C. The mobile phase consisted of 0.1% formic acid (solvent A) and acetonitrile (solvent B), delivered in gradient elution mode at a flow rate of 0.45 ml/min. The following program was applied: isocratic 5% B for 1 min, 5% to 95% B over 5 min, isocratic 95% B for 2 min, 95% to 5% B over 1 min, isocratic 5% for 4 min. Modified nucleosides were detected using nucleoside-to-base ion transitions as follows: 268 → 136 (A); 282 → 136 (Am); 284 → 152 (G); 298 → 152 (Gm); 244 → 112 (C); 258 → 112 (Cm); 245 → 113 (U); 259 → 113 (Um); 282 → 150 (m6A); 296 → 150 (m6Am); 269 → 137 (I); 283 → 137 (Im); and 247 → 115 (DHU). The interface temperature was set to 300°C, and the desolvation line was set to 250°C. Nitrogen was used as the nebulizing (3 l/min) and drying (10 l/min) gas, and dry air was used for heating (10 l/min). Data acquisition and analysis were performed using LabSolutions LCMS software v5.82 SP1 (Shimadzu, Japan). For relative quantification, the peak areas of 2'-O-methylated nucleosides in RNA hydrolysates and free nucleoside extracts were normalized to the corresponding unmodified nucleosides. Additionally, peak areas of all modified and unmodified nucleosides in free nucleoside extracts were normalized to the dihydrouridine (DHU) to enable sample-to-sample comparison.

Statistical analysis

Statistical significance was assessed using unpaired two-tailed *t*-tests with the Welch correction, with an alpha level of 0.05. Error bars in the figures represent the standard error of the mean (SEM), and values following the ± symbol indicate the SEM. All statistical analyses were performed using GraphPad Prism v8.4.

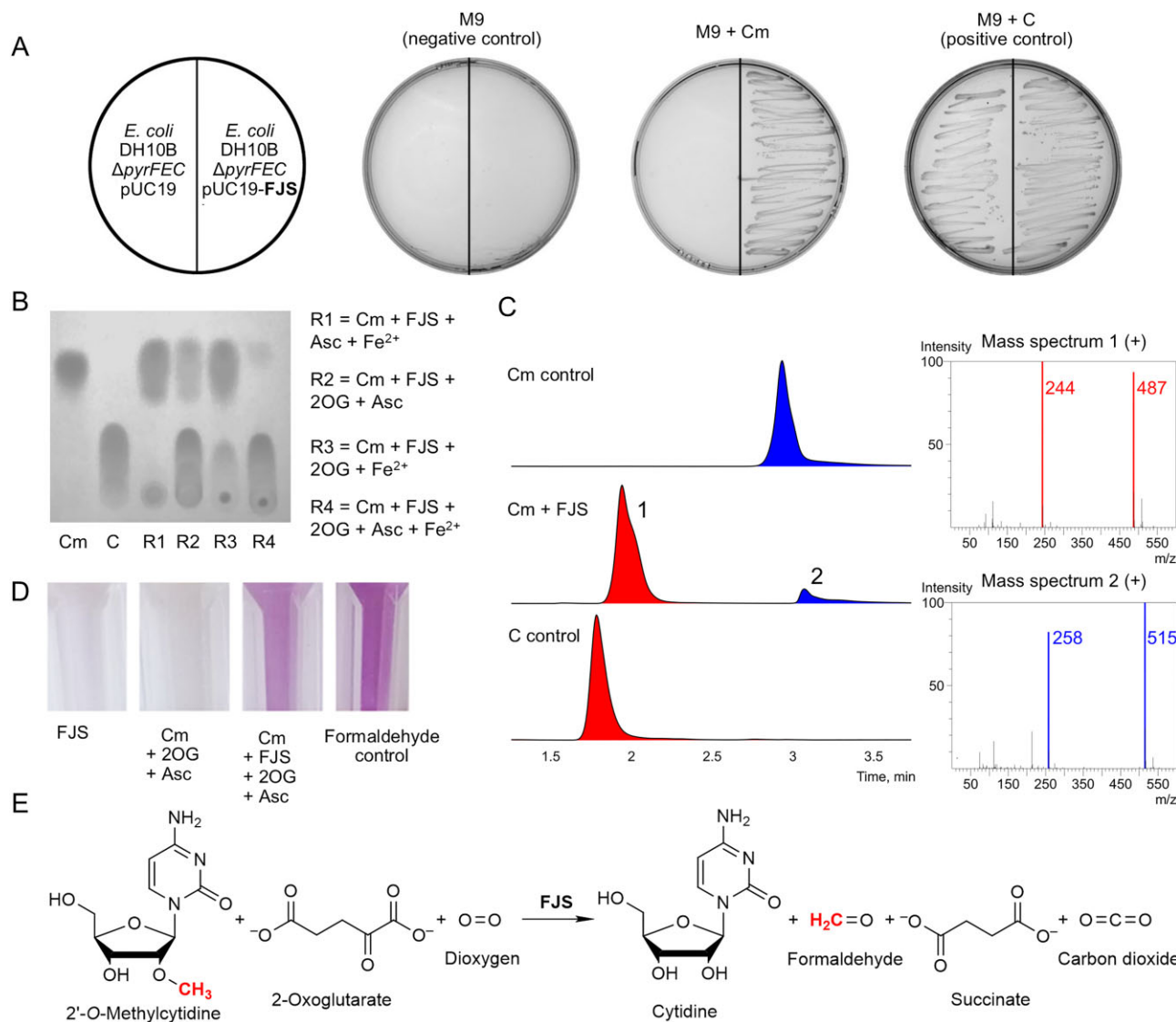


Figure 1. Discovery and characterization of FJS catalytic activity. **(A)** The functionality of FJS, encoded in the pUC19 vector, was identified using the *E. coli* DH10B Δ pyrFEC strain. **(B)** The enzymatic activity of FJS depends on 2-oxoglutarate and is further enhanced *in vitro* by adding ascorbate and FeSO₄. **(C)** HPLC-MS analysis confirmed the loss of the methyl group during the reaction by detecting a 14 Da decrease in the mass of 2'-O-methylcytidine. **(D)** The methyl group from the modified nucleoside is converted to formaldehyde, as demonstrated by the reaction with Purpald reagent. **(E)** Proposed reaction scheme for the FJS-catalyzed demethylation of 2'-O-methylcytidine. Cm, 2'-O-methylcytidine; C, cytidine; 2OG, 2-oxoglutarate; Asc, ascorbate.

Results

Identification of a novel 2'-O-methyl nucleoside demethylation reaction

Our previous studies have shown that auxotrophic complementation-based selection is an effective method for identifying novel enzymes, including those misannotated in various databases [43, 44, 61–63]. This study aimed to identify novel enzymes involved in the catabolism of 2'-O-methyl nucleosides by further screening our metagenomic libraries. Therefore, we transformed an auxotrophic *E. coli* DH10B Δ pyrFEC strain, which requires uridine (uracil) or cytidine (cytosine) for growth, with various metagenomic libraries. Positive hits were selected on a mineral medium supplemented with 2'-O-methylcytidine—a compound that this particular *E. coli* strain cannot naturally metabolize—as the sole pyrimidine nucleoside source. Consequently, the transformed bacteria could only grow if they carried a plasmid

encoding a protein capable of degrading 2'-O-methylcytidine into cytidine or cytosine (Fig. 1A).

Using this approach, we isolated plasmid DNA (pUC-19-FJS) containing an ~1200 bp insert from the soil-based F21,23/BamHI library. Sequence analysis revealed that the insert is likely to be of bacterial origin and includes an 858 bp open reading frame (ORF) encoding a novel 2-oxoglutarate and iron(II)-dependent dioxygenase with a predicted molecular mass of 32.0 kDa, which we designated FJS. Protein sequence analysis using the NCBI database [64] and blastx [65] identified the closest known sequences as a phytanoyl-CoA dioxygenase family protein from *Labrys monachus* (85.05% identity, WP_307431252.1) and an unclassified *Acidisoma* (77.82% identity, WP_158801103.1). Other sequences highly similar to FJS are also of bacterial origin, such as *Dongiaceae*, *Roseiarcus*, *Gemmamimonadota*, and *Candidatus Poribacteria*.

Table 1. Substrate scope of FJS and the human PHYHD1 isoform A *in vitro*

Substrate	FJS activity <i>in vitro</i>	Human PHYHD1 isoform A activity <i>in vitro</i>	Product
2'-O-Methylcytidine	+++	++++	Cytidine
2'-O-Methyluridine	+++	++++	Uridine
2'-O-Methyladenosine	+++	++++	Adenosine
N ⁶ ,2'-O-Dimethyladenosine	+++	++++	N ⁶ -Methyladenosine
2'-O-Methylguanosine	++	++++	Guanosine
2'-O-Methylinosine	++	++	Inosine
2'-O-Methyl-5-methylcytidine	++++	++	5-Methylcytidine
N ⁴ ,2'-O-Dimethylcytidine	+++	++++	N ⁴ -Methylcytidine
N ⁴ -Acetyl-2'-O-methylcytidine	++	++	N ⁴ -Acetylcytidine
N ⁴ -Benzoyl-2'-O-methylcytidine	++	++	N ⁴ -Benzoylcytidine
2'-O-Methyl-5-methyluridine	+++	+	5-Methyluridine
2'-O-Methyl-5-fluorouridine	+++	++++	5-Fluorouridine
2'-O-Allyluridine	+	+	Uridine
2'-O-Methylcytidine 5'-monophosphate*	-	-	-
2'-O-Methyluridine 5'-monophosphate*	-	-	-
2'-O-Methyladenosine 5'-monophosphate*	-	-	-
2'-O-Methylguanosine 5'-monophosphate*	-	-	-
2'-O-Methylcytidine 5'-triphosphate	-	-	-
2'-O-Methyluridine 5'-triphosphate	-	-	-
2'-O-Methyladenosine 5'-triphosphate	-	-	-
2'-O-Methylguanosine 5'-triphosphate	-	-	-
3'-O-Methyluridine	-	-	-
3'-O-Allyluridine	-	-	-
2',3'-O-Isopropylideneuridine	-	-	-

Reaction mixtures for qualitative assays contained 15–80 μ M purified oxygenase, 5 mM substrate (except 1 mM N⁴-benzoyl-2'-O-methylcytidine, 10 mM 2-oxoglutarate, 0.5 mM FeSO₄, and 1 mM ascorbate in 50 mM Tris-HCl (pH 8.0)). Reactions were conducted at 37°C for 1 h, or at 30°C for 2 h or overnight, then quenched with an equal volume of acetonitrile. For quantitative analysis, reactions were performed with 10 μ M enzyme (based on active sites, 0.33 mg/ μ l) and 1 mM substrate at 37°C for 30 min. After quenching, reaction mixtures were analysed by HPLC-MS. Demethylation efficiency is indicated as follows: ++++ 90–100% substrate conversion, +++ 70–90%, ++ 40–70%, + 20–40%. Compounds marked with an asterisk (*) were tested as mixtures with their corresponding nucleosides and were synthesized using *D. melanogaster* deoxynucleoside kinase, as described in the Materials and methods.

The gene encoding FJS was cloned into the pLATE31 vector with a C-terminal His-tag (GHIIHHHHG, protein sequence available in *Supplementary Table S2*). This was followed by overexpression in *E. coli* HMS174(DE3), nickel affinity chromatography, and desalting via size exclusion chromatography, as overnight dialysis resulted in an inactive protein. Gel filtration chromatography of FJS revealed an elution volume corresponding to a protein with a molar mass of ~71 kDa (*Supplementary Fig. S1*). This suggests that FJS may function as a dimer, as the theoretical molar mass of two His-tagged monomers is 65.84 kDa. The observed 5 kDa discrepancy could be attributed to nucleic acid fragments bound to the purified protein, as nucleic acid contamination was detected in the sample (*Supplementary Fig. S2A*). To investigate this, nucleic acid purification was performed on recombinant FJS using Proteinase K treatment, followed by phenol extraction and enzymatic analysis with DNase I and RNase A (*Supplementary Fig. S2B*). The result showed that both RNA and DNA were bound to purified FJS, suggesting that during purification from *E. coli*, recombinant FJS interacts with nucleic acids in a non-specific manner.

To determine the precise reaction catalyzed by FJS, we analysed the enzymatic activity of purified recombinant protein using TLC, HPLC-MS, and Purpald reagent (Fig. 1B, C, D). Our results revealed that the enzyme catalyzes a novel biodegradation pathway for 2'-O-methylcytidine, in which FJS removes the 2'-O-methyl group, yielding cytidine and formaldehyde. This reaction requires 2-oxoglutarate as a co-substrate, and the efficiency of FJS is further enhanced by Fe(II) ions and ascorbate, resembling the behaviour of typical 2OG oxygenases [66]. HPLC-MS analysis confirmed that during the reaction, the mass of 2'-O-methylcytidine decreased by 14 Da

(from 258 to 244 Da), consistent with the loss of the methyl group. The proposed mechanism suggests that FJS first oxidizes the 2'-O-methyl group with molecular oxygen, forming an unstable intermediate that spontaneously degrades into cytidine and formaldehyde. Simultaneously, 2-oxoglutarate is converted to succinate and CO₂ (Fig. 1E).

We then tested FJS activity against a range of modified nucleosides, nucleotides, and phytanoyl-CoA to further explore its substrate specificity. FJS showed no catalytic activity toward 2'-O-methylated nucleoside monophosphates, triphosphates, or nucleosides modified at the 3'-O position (Table 1), and only produced a negligible trace quantity of hydroxylated phytanoyl-CoA (*Supplementary Fig. S3*). The highest activity was observed with 2'-O-methyl-5-methylcytidine ($k_{cat} = 0.110 \pm 0.008/s$, $K_m = 0.889 \pm 0.136$ mM at 30°C, 1.0 mg/ml enzyme concentration) compared with 2'-O-methylcytidine ($k_{cat} = 0.040 \pm 0.003/s$, $K_m = 0.525 \pm 0.101$ mM, *Supplementary Fig. S4*). The lowest FJS activity was observed with 2'-O-allyluridine. Interestingly, although the nucleobase influenced demethylation efficiency to some extent, FJS consistently targeted the 2'-O modification regardless of base size (e.g. N⁴-benzoyl cytidine) or modification length (e.g. allyl versus methyl), demonstrating broad substrate specificity.

FJS exhibited optimal activity in HEPES-KOH (pH 7.3) and Tris-HCl (pH 7.5 at 37°C, equivalent to pH 8.0 at room temperature), with the highest demethylation efficiency observed at 50°C (*Supplementary Fig. S5*). However, similar to many other 2OG oxygenases [67], FJS rapidly loses activity over time. After 6 h of incubation, its enzymatic activity decreased by 14.5% at 4°C, 53.8% at 20°C, 91.3% at 30°C, and 95.0% at 37°C (*Supplementary Fig. S6*).

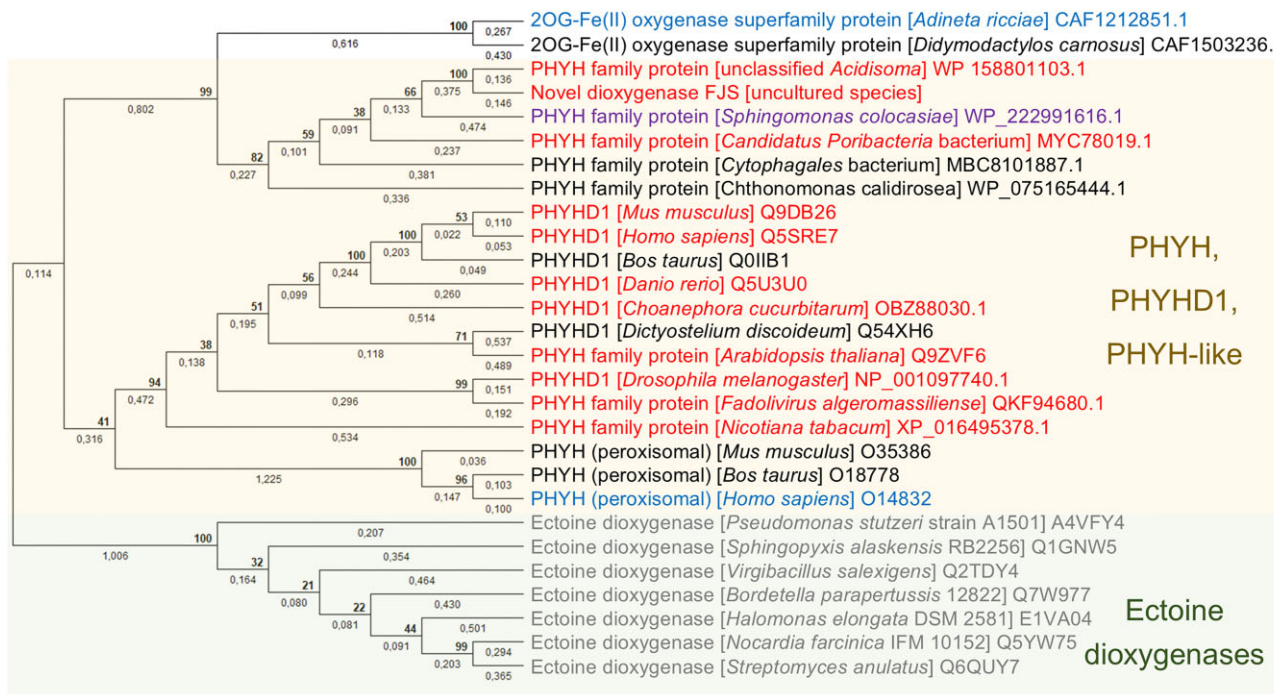


Figure 2. Evolutionary analysis of representative phytanoyl-CoA dioxygenase (PHYH), PHYH domain-containing 1 (PHYHD1), and other related protein sequences. Dioxygenases marked in red exhibited *in vitro* 2'-O-methyl nucleoside demethylation activity when tested with 2'-O-methyluridine, 2'-O-methylcytidine, 2'-O-methyladenosine, and 2'-O-methylguanosine. The enzyme shown in purple displayed activity exclusively toward 2'-O-methylguanosine *in vitro*, whereas those marked in blue were tested but showed no detectable demethylation activity.

2'-O-Methyl nucleoside demethylase FJS is related to human PHYHD1

Phylogenetic analysis of the FJS amino acid sequence revealed its close relationship to bacterial ectoine dioxygenases and its significant similarity to enzymes belonging to or resembling the phytanoyl-CoA dioxygenase family proteins (Fig. 2). Furthermore, an evolutionary analysis of all reviewed 2-oxoglutarate-dependent dioxygenase sequences from the UniProtKB dataset [47] placed FJS within the same clade as phytanoyl-CoA dioxygenase domain-containing 1 (PHYHD1) dioxygenases (Supplementary Tree). This finding was particularly intriguing, as the physiological substrate for PHYHD1 hydroxylation had not yet been identified, as noted in the Introduction. Given its sequence similarity to FJS, we hypothesized that dioxygenases annotated as PHYHD1, or other proteins belonging to the phytanoyl-CoA dioxygenase family, may function as 2'-O-Me nucleoside demethylases.

To test this hypothesis, we synthesized genes encoding selected members of the phytanoyl-CoA dioxygenase family and related 2OG-Fe(II) oxygenases, and cloned them into the pET-21 expression vector (protein sequences available in Supplementary Table S2). The chosen proteins included the closest bacterial homologs as well as animal, plant, fungal, and viral variants. In addition, two genes encoding different isoforms of *D. rerio* (zebrafish) PHYHD1 were amplified from cDNA and cloned into pLATE31 expression vectors (isoform X1 is longer by two amino acids, Q64 and M65).

Using these constructs, we evaluated whether *in vivo* expression of the selected dioxygenases could complement the *E. coli* HMS174(DE3) Δ pyrF strain grown on medium supplemented with 2'-O-methylcytidine (Fig. 3) or 2'-O-methyluridine (Supplementary Fig. S7). All tested animal (fruitfly, zebrafish, mouse, and human) and fun-

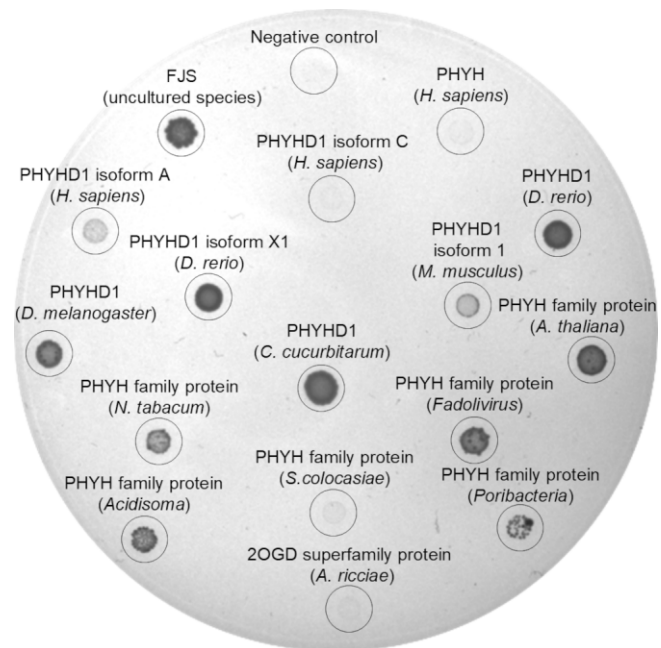


Figure 3. Phytanoyl-CoA dioxygenase family demethylation activity was demonstrated by complementation of the uridine/cytidine auxotrophic *E. coli* HMS174(DE3) Δ pyrF strain after 1 week of growth at room temperature. Tested dioxygenases were expressed from either pET-21 or pLATE31 vectors. The abbreviated names of the oxygenases are indicated above the respective colonies. M9 medium was supplemented with 10 mg/l 2'-O-methyluridine.

gal (*Choanephora cucurbitarum*) dioxygenases, classified as PHYHD1, exhibited 2'-O-methylcytidine demethylase activ-

ity. Furthermore, enzymes from plants (*Arabidopsis thaliana* and *Nicotiana tabacum*), bacteria (*Sphingomonas*, *Poribacteria*, and *Acidisoma*), and a virus (*Fadolivivirus algeromasiliense*, an amoeba virus with a 1.5 Mb genome [68])—all annotated as phytanoyl-CoA dioxygenase family members—also complemented the HMS174(DE3) Δ pyrF strain. These results indicate that demethylase activity is widespread within this enzyme family (PF05721). Notably, no activity toward 2'-O-Me nucleosides was detected for human phytanoyl-CoA dioxygenase, suggesting a distinct substrate specificity.

To confirm that dioxygenases complementing the HMS174(DE3) Δ pyrF strain also exhibit demethylation activity *in vitro*, we first purified the corresponding His-tagged enzymes from *E. coli* LOBSTR cells using nickel affinity chromatography. After purification, the enzymes were desalted using size exclusion chromatography, as overnight dialysis led to enzyme inactivation, as was observed for FJS (purified protein PAGE analysis is provided in *Supplementary Fig. S8*). All dioxygenases that complemented the *E. coli* HMS174(DE3) Δ pyrF strain demonstrated *in vitro* activity on 2'-O-methylated nucleosides.

We also observed that *E. coli* HMS174(DE3) Δ pyrF cells expressing human PHYHD1 isoform A (hPHYHD1) exhibited reduced growth compared with those expressing FJS or other PHYHD1 dioxygenases. However, purified hPHYHD1 isoform A showed higher *in vitro* activity, with greater efficiency toward purine-based nucleosides than pyrimidine-based ones (Table 1). Specifically, the initial product formation rates were 0.049 mM/min for 2'-O-methyladenosine, 0.038 mM/min for 2'-O-methylguanosine, 0.027 mM/min for 2'-O-methylcytidine, and 0.016 mM/min for 2'-O-methyluridine, with 1 mM initial substrate concentration and 10 μ M purified recombinant hPHYHD1 isoform A. Additionally, hPHYHD1 isoform C was inactive in both *E. coli* HMS174(DE3) Δ pyrF and *in vitro*, as previously predicted [31].

Bioinformatics analysis indicates that all tested 2'-O-Me nucleoside demethylases contain the conserved catalytic domain characteristic of 2OG oxygenases (*Supplementary Fig. S9*). This domain features a distorted double-stranded β -helix (DSBH) core fold, composed of eight β -strands arranged into two β -sheets: a major sheet (strands I, III, VI, and VIII) and a minor sheet (strands II, IV, V, and VII), which together form a squashed barrel with an opening accommodating the Fe(II)- and 2OG-binding sites [27]. As is typical for 2OG oxygenases [27], the active site triad consists of a proximal histidine on the β -II strand, followed by asparagine and aspartate residues, and a distal histidine on the β -VII strand (H-X-D...H motif). The primary structural difference between human PHYH and PHYHD1 lies in the size of the active site cavity (1296.86 \AA^3 in the hPHYH AlphaFold-predicted structure versus 627.26 \AA^3 in the hPHYHD1 crystal structure) and the presence of an additional α -helix near the cavity opening (residues Q56–L71, denoted α 4 in *Supplementary Fig. S9* and highlighted in red in *Supplementary Fig. S10c*). This α -helical element has previously been identified as a unique structural feature of PHYHD1, distinguishing it from other 2OG oxygenases [31]. Interestingly, the predicted structure of FJS also contains two shorter α -helices near the active site cavity opening (*Supplementary Fig. S9*), but these are formed by C-terminal residues (R264–G271, V278–Q284). Similar structural features are observed in other PHYH-like 2'-O-Me nucleoside demethylases, such as those from *Arabidopsis* and *Fadolivirus* (*Supplementary Fig. S9*).

Docking of 2'-O-methylated nucleosides to the active centre of the human PHYHD1 isoform

A crystal structure [31], using the Attracting Cavities 2.0 [55] algorithm, yielded high-scoring configurations that consistently positioned the nucleoside ribose moiety towards the active site iron. In the cases where the lowest ΔG_{SP} values were achieved (Fig. 4), the 2'-O-Me group points directly toward the active centre iron, with a distance of 4.087 \AA for 2'-O-methyladenosine and a distance of 4.295 \AA for 2'-O-methylcytidine between the 2'-O-Me group carbon atom and the iron ion. The ribose ring is coordinated by hydrogen bonds with the side chains of lysine (K102), histidine (H105), glutamine (Q139), and tryptophan (W277)—all conserved among the tested non-bacterial demethylases (*Supplementary Fig. S9*). The nucleobase is stabilized through π - π stacking with semi-conserved phenylalanine (F161), which is replaced by tyrosine in bacterial demethylases. Interestingly, purine bases are further stabilized by a hydrogen bond with serine (S154), whereas pyrimidine bases lack this interaction. This difference, together with the stronger π - π interactions between the phenylalanine ring and purines compared with pyrimidines, probably underlies the higher activity of hPHYHD1 toward 2'-O-methylated purine nucleosides. Moreover, the docking results offer an explanation for why hPHYHD1 is inactive towards 2'-O-Me nucleoside 5'-phosphates and 3'-O-modified nucleosides: the presence of a 5'-phosphate group probably introduces steric hindrance, and therefore the 3'-O-methyl group is positioned too far from the catalytic centre iron to allow efficient demethylation.

Human PHYHD1 and plant PHYH-like dioxygenases do not demethylate miR173/miR173*^{CH3} duplexes

To investigate whether 2'-O-methyl nucleoside demethylases are capable of removing 2'-O-methyl groups from nucleic acids, we first tested our bacterial demethylase FJS activity on methylated single-stranded RNA (miR173^{CH3}) and methylated RNA/RNA or RNA/DNA duplexes (miR173^{CH3}/miR173* or miR173^{CH3}/DNA), but observed no activity (*Supplementary Fig. S11*). After experiment optimization, we decided to focus on investigating whether hPHYHD1 and other PHYH-like dioxygenases could also act on 2'-O-methyl ribose moieties within an RNA chain. Therefore, we tested human and plant PHYHD1 homologs on a methylated miRNA duplex (miR173/miR173*^{CH3}) with 2 nt 3'-overhangs. This duplex, naturally methylated by the small RNA methyltransferase HEN1 in *A. thaliana* [69], carries a 3'-terminal 2'-O-methylguanosine on the miR173*^{CH3} strand (Fig. 5B). If demethylated by an oxygenase, the RNA molecule would become susceptible to periodate treatment, as observed with the unmethylated miR173/miR173* control (Fig. 5A). The absence of truncated products following incubation with the enzymes indicated that 3'-terminal 2'-O-methylated miRNA is not a suitable substrate for the selected human and plant demethylases *in vitro*. Similar results were obtained using methylated miR173^{CH3}/miR173*, which carries a 3'-terminal 2'-O-methylated cytidine (data not shown). Combined with the observation that FJS and human PHYHD1 were also inactive towards ribose-methylated nucleoside monophosphates and triphosphates, our findings suggest that these dioxygenases specifically target free nucleosides rather than those incorporated into RNA. Nonetheless, given that PHYHD1 dysregulation has been linked to abnormal

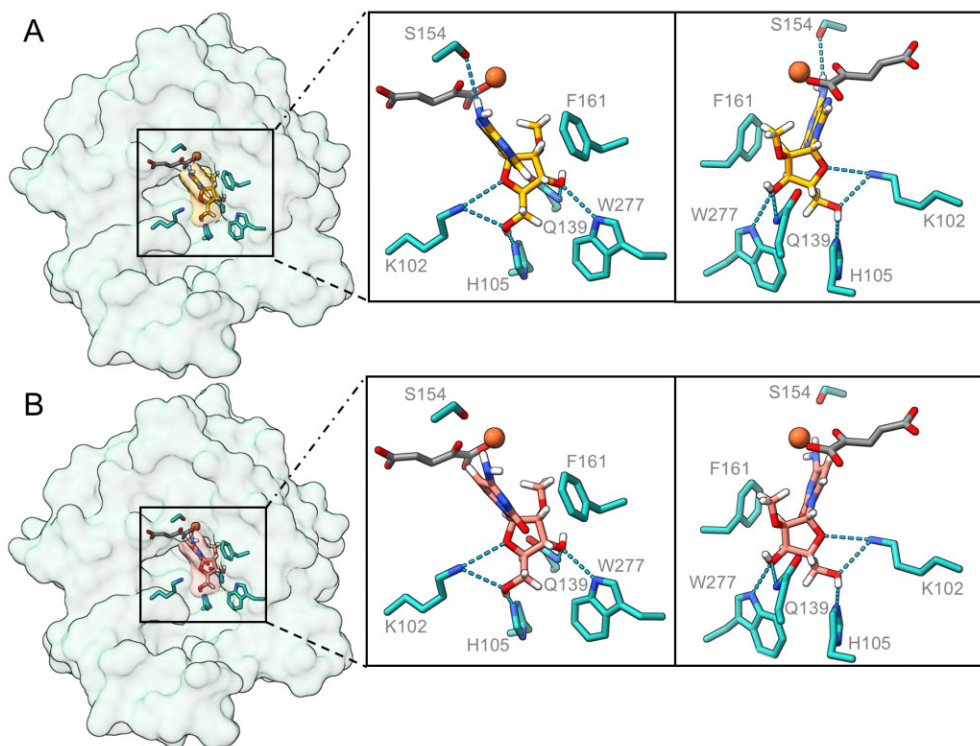


Figure 4. Molecular docking of 2'-O-methyladenosine (A, yellow) and 2'-O-methylcytidine (B, salmon pink) on the PHYHD1 crystal structure (PDB ID: 30BZ) [31] using the Attracting Cavities 2.0 algorithm [55]. Docking results with the lowest ΔG_{SP} values (-7.0663 for 2'-O-methyladenosine and -6.9917 for 2'-O-methylcytidine) are shown. The active centre iron ion is depicted as orange, and 2-oxoglutarate is depicted as grey.

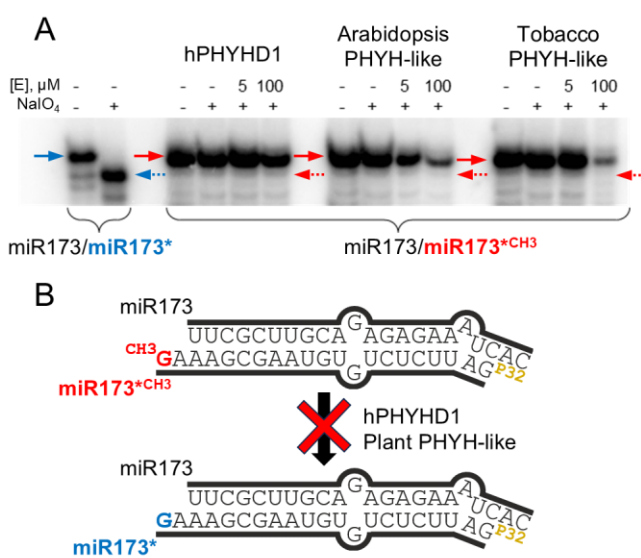


Figure 5. miRNA 3'-terminal demethylation assay. Sodium periodate (NaIO_4)-mediated oxidation followed by β -elimination (A) shows that human PHYHD1 and plant PHYH-like demethylases do not remove the 2'-O-methyl group from the miR173/miR173*^{CH3} duplex (B). Solid arrows indicate full-length RNA strands. The dotted arrows point to the position of the unmethylated strand truncated by β -elimination. Reaction mixtures contained $0.1 \mu\text{M}$ RNA duplex, 5 or $100 \mu\text{M}$ oxygenase, 10 mM 2-oxoglutarate, 1 mM ascorbate, and 0.25 mM FeSO_4 in 50 mM Tris-HCl, pH 8.0. Incubation was performed for 4 h at 30°C , followed by periodate treatment.

physiological states and that hPHYHD1 has been shown to interact with RNA *in vitro* [30], the possibility remains that these demethylases require additional enzymes or specific physiological conditions to act on RNA substrates *in vivo*. Alternatively, PHYHD1 could indirectly influence RNA 2'-O-methylation levels by playing a specific role in the catabolism of modified nucleosides. Thus, to further investigate the *in vivo* role of PHYHD1, we selected zebrafish (*D. rerio*) as a model organism.

Knocking out the *phyhd1* gene does not influence RNA 2'-O-Me levels in zebrafish

To determine whether PHYHD1 influences RNA 2'-O-methylation levels *in vivo*, we generated a zebrafish *phyhd1*-KO mutant line (*vln31*) using CRISPR/Cas9 gene editing technology. The targeted region included the first two amino acids of the active site triad—proximal histidine H156 and an active site aspartate D158 (Supplementary Fig. S12)—to ensure that the resulting gene product was inactive. Injection of the CRISPR components into 1-cell stage AB strain WT zebrafish embryos produced F_0 mosaic mutants, which were then outcrossed to generate F_1 heterozygous mutants. Subsequent in-crossing of F_1 fish yielded F_2 homozygous *phyhd1*-KO embryos. Adult F_2 *phyhd1*-KO ($n = 5$; 3 female, 2 male) and F_3 embryos exhibited no apparent differences in morphology or viability compared with controls.

When grown in the same tank as WT fish ($n = 60$, 30 *phyhd1*-KO and 30 WT embryos) up to 100 dpf, the F_3 *phyhd1*-KO mutant line showed a slight reduction in survivability, with 17 *phyhd1*-KO embryos reaching adulthood com-

pared with 23 WT. However, no significant differences were observed in standard length (18.4 ± 0.4 mm for *phyhd1*-KO versus 17.5 ± 0.3 mm for WT males) or body weight (76.2 ± 4.4 mg for *phyhd1*-KO versus 68.9 ± 3.0 mg for WT males). Nevertheless, a notable disparity in sex ratio was observed: only one *phyhd1*-KO zebrafish (5.9%) developed as female, compared with 39.1% females among WT fish raised in the same tank. This lone *phyhd1*-KO was also the smallest in the tank (13.8 mm versus 18.1 ± 0.55 mm for WT females) and had the lowest weight (32 mg versus 91.7 ± 8.8 mg for WT females). A follow-up experiment with 30 combined embryos (15 *phyhd1*-KO and 15 WT) yielded similar results: 11 *phyhd1*-KO and 15 WT survived until sexual maturity, and the sex ratio again differed (18.2% female among *phyhd1*-KO versus 55.6% female among WT). However, in this cohort, the two *phyhd1*-KO females did not differ significantly from WT females in length (14.9 ± 0.9 mm *phyhd1*-KO versus 13.9 ± 3.7 mm WT) or weight (49.5 ± 8.5 mg *phyhd1*-KO versus 63.2 ± 25.1 mg WT). These findings suggest that PHYHD1 may play a minor role in zebrafish sex determination. Nevertheless, zebrafish are known for highly variable sex ratios, which can shift markedly in either direction within as few as three generations [70]. Therefore, further investigation is needed to establish any definitive role of PHYHD1 in this process.

As no visible phenotypic differences were observed in the F_2 and F_3 generations, we analysed RNA 2'-O-methylation levels in WT and *phyhd1*-KO embryos and adult fish (Fig. 6). However, no statistically significant changes were detected. The most notable relative difference was observed in the Am/A ratios (0.00251% *phyhd1*-KO versus 0.00149% WT).

Loss of PHYHD1 function significantly increases the levels of free 2'-O-methylated nucleosides

With no difference found in RNA modification levels, we next examined free 2'-O-methylated nucleosides, which are not incorporated into the structure of RNA or other (macro)molecules. To quantify these nucleosides, zebrafish WT and *phyhd1*-KO embryos and adults were first digested with proteinase K. Ice-cold acetonitrile was then used to precipitate unwanted macromolecules, and the resulting soluble supernatant was analysed by HPLC-MS/MS. This analysis revealed significant increases in all Nm/N ratios in mutant zebrafish embryos and adults compared with the WT, except for the 2'-O-methyladenosine/adenosine ratio, which exhibited only a slight elevation (Fig. 7). The minor change for 2'-O-methyladenosine can be attributed to its rapid deamination and accumulation as 2'-O-methylinosine.

As shown in Fig. 7, in the case of purine bases, the Im/I ratio increased ~ 20 -fold in mutant embryos and 35-fold in adults, while the Gm/G ratio increased 100-fold in embryos and 35-fold in adults. For pyrimidine bases, the Cm/C ratio increased 45-fold in embryos and 10-fold in adults, while the Um/U ratio increased >125 -fold in embryos and 45-fold in adults.

When normalized to the dihydrouridine (DHU) signal, statistically significant increases were observed for 2'-O-methylinosine (+1736% in embryos, +3364% in adults), 2'-O-methylguanosine (+6764% in embryos, +3754% in adults), 2'-O-methylcytidine (+2302% in embryos, +800% in adults), and 2'-O-methyluridine (+6972% in embryos, +6330% in adults), with 2'-O-methyluridine showing the

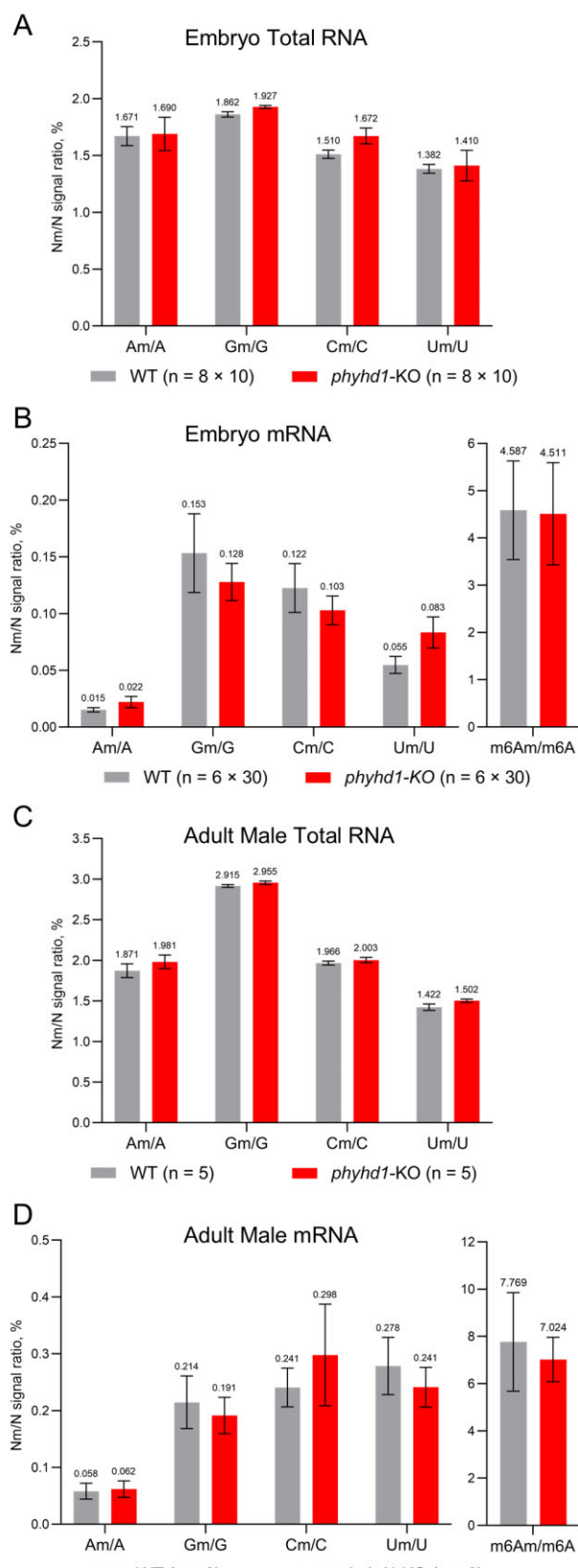


Figure 6. Relative levels of 2'-O-methylated nucleosides (Nm) compared with unmodified nucleosides (N) in total RNA (A, C) and mRNA (B, D) purified from WT and *phyhd1*-KO zebrafish embryos (24 h post-fertilization) and adult males (3 months post-fertilization). Data represent means \pm SEM from at least five biological replicates.

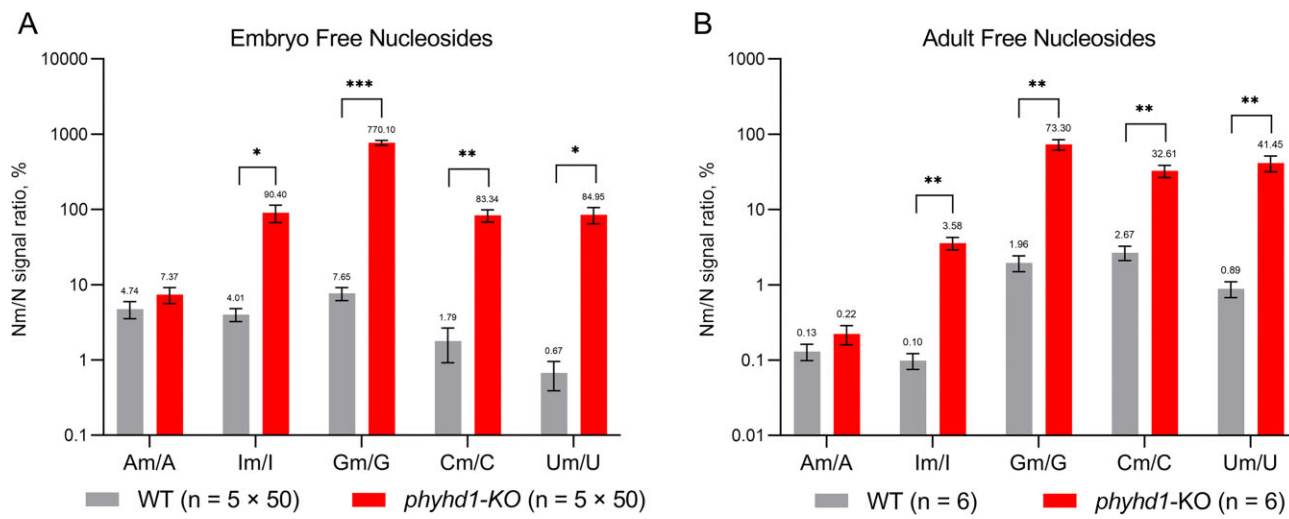


Figure 7. Relative levels of free 2'-O-methylated nucleosides (Nm) compared with unmodified nucleosides (N) in extracts from WT and *phyhd1*-KO zebrafish embryos (A) and adult zebrafish (B). Embryos were collected 24 h post-fertilization, and adult zebrafish (five each WT and *phyhd1*-KO males and three each WT and *phyhd1*-KO females) were collected 3 months post-fertilization. Data represent means \pm SEM from at least three biological replicates. Statistical significance was determined using unpaired two-tailed *t*-tests with Welch correction; *P*-values are indicated as follows: ns, *P* > 0.05; **P* ≤ 0.05; ***P* ≤ 0.01; ****P* ≤ 0.001.

largest relative increase (Table 2). A substantial but statistically non-significant increase was also observed for 2'-O-methyladenosine (+56% in embryos and +29% in adults). These data indicate that free 2'-O-methyl nucleosides are the primary physiological substrates of PHYHD1.

Interestingly, zebrafish embryos showed lower unmodified N/DHU ratios, suggesting that the accumulation of 2'-O-methyl nucleosides might also impede the turnover of unmodified nucleosides. This effect could, however, be partly due to elevated DHU levels, as it was less pronounced in adult zebrafish. Additionally, it may be amplified in embryos because they have reduced metabolite exchange with the environment and have not yet begun ingesting nucleoside- or nucleoside-derivative-containing food.

Collectively, these findings demonstrate that, in zebrafish, PHYHD1 primarily functions in the demethylation of free 2'-O-methyl nucleosides, facilitating their turnover and preventing excessive accumulation.

Discussion

In this study, we demonstrate that PHYHD1 and homologous dioxygenases—found across all domains of life, including bacteria, fungi, plants, invertebrates, vertebrates, mammals, and even a virus—function as 2'-O-methylated nucleoside demethylases. The ubiquity of this enzymatic activity suggests its potential biological importance in modulating 2'-O-methylated nucleosides, which are found in virtually all classes of RNA. However, a crucial question remains: does PHYHD1 demethylate RNA?

Our findings suggest that PHYHD1 does not act on 2'-O-methylated nucleosides incorporated into RNA. The lack of detectable activity on methylated miRNA, as well as on mono- and triphosphorylated 2'-O-Me nucleosides, indicates that PHYHD1 probably does not target structured RNA molecules. This is further supported by our *in vivo* data, which show that *phyhd1*-KO zebrafish embryos and adults exhibit no significant changes in overall RNA 2'-O-Me levels. These observations suggest that PHYHD1 may not be involved

in global RNA demethylation. However, the possibility that PHYHD1 acts on specific RNA targets or only functions under particular cellular conditions, such as during splicing or RNA processing, remains. Previously, Ala-Nisula and colleagues reported that human PHYHD1 does not demethylate an 18S RNA oligonucleotide containing 2'-O-methylcytidine but binds mRNA more strongly than rRNA and interacts with the spliceosome and proteins involved in RNA splicing [30]. This suggests that PHYHD1 may play a more nuanced role in RNA metabolism, potentially influencing RNA modification indirectly rather than serving as a direct RNA demethylase.

Despite the lack of direct evidence for RNA demethylation, the identification of 2'-O-methylated nucleosides as primary substrates of PHYHD1 opens up new avenues for further studies. Indeed, understanding the biological function of PHYHD1 is of great importance, given its implication in various human diseases. Previous studies have shown that human PHYHD1 expression negatively correlates with 2'-O-methyluridine and 2'-O-methylcytidine levels in plasma and cerebrospinal fluid [71]. Furthermore, genome-wide association studies of human metabolites (data available through the NHGRI-EBI GWAS Catalog [72]) have linked single-nucleotide polymorphisms in the PHYHD1 gene to altered levels of 2'-O-methylcytidine and 2'-O-methyluridine (Supplementary Table S3). These findings support the notion that PHYHD1 contributes to the turnover of 2'-O-methylated nucleosides in humans, a function analogous to its role in zebrafish.

Although zebrafish PHYHD1 (and probably other 2'-O-methyl nucleoside demethylases) does not appear to directly modulate RNA 2'-O-methylation, the accumulation of free 2'-O-methylated nucleosides could have meaningful physiological consequences. For example, 2'-O-methylcytidine 5'-triphosphate, a phosphorylated derivative of 2'-O-methylcytidine, is a known inhibitor of viral RNA-dependent RNA polymerases [73], illustrating the ability of these modified nucleotides to interfere with polymerase activity. By analogy, the absence of functional PHYHD1, re-

Table 2. Relative levels of free 2'-O-methylated nucleosides (Nm) and unmodified nucleosides (N) normalized to DHU, in extracts from WT and *phyhd1*-KO zebrafish

Sample	Nucleoside	WT N(m)/DHU	<i>phyhd1</i> -KO N(m)/DHU	Relative change	P-value
Embryo	A	53.5 ± 11.6	25.2 ± 6.71	-53%	ns
Embryo	Am	1.25 ± 0.286	1.952 ± 0.782	+56%	ns
Embryo	I	31.6 ± 7.41	21.8 ± 1.86	-31%	ns
Embryo	Im	0.997 ± 0.334	18.3 ± 3.19	+1736%	**
Embryo	G	7.03 ± 2.67	2.10 ± 0.144	-70%	ns
Embryo	Gm	0.233 ± 0.0543	16.0 ± 1.28	+6764%	***
Embryo	C	28.0 ± 8.37	11.9 ± 1.73	-58%	ns
Embryo	Cm	0.373 ± 0.0981	8.95 ± 0.824	+2302%	***
Embryo	U	9.47 ± 3.00	3.74 ± 0.372	-60%	ns
Embryo	Um	0.0488 ± 0.0132	3.45 ± 1.18	+6972%	*
Adult	A	538 ± 117	492 ± 115	-9%	ns
Adult	Am	0.620 ± 0.139	0.800 ± 0.0878	+29%	ns
Adult	I	777 ± 157	626 ± 183	-19%	ns
Adult	Im	0.613 ± 0.0797	21.2 ± 6.27	+3364%	*
Adult	G	38.6 ± 9.78	38.5 ± 13.8	-0.3%	ns
Adult	Gm	0.556 ± 0.0815	21.4 ± 6.44	+3754%	*
Adult	C	44.4 ± 10.7	59.6 ± 24.7	+34%	ns
Adult	Cm	0.903 ± 0.111	8.13 ± 0.929	+800%	***
Adult	U	14.4 ± 2.22	15.9 ± 1.82	+10%	ns
Adult	Um	0.109 ± 0.0155	7.02 ± 2.08	+6330%	*

Embryos (24 hpf; WT $n = 5 \times 50$, *phyhd1*-KO $n = 5 \times 50$), adult zebrafish (3 months post-fertilization; WT $n = 6$, *phyhd1*-KO $n = 6$; each group comprised three males and three females) were analyzed. Data are represented as means ± SEM from at least three biological replicates. Statistical significance was assessed using unpaired two-tailed *t*-tests with Welch correction; *P*-values are indicated as follows: ns, *P* > 0.05; **P* ≤ 0.05; ***P* ≤ 0.01; ****P* ≤ 0.001.

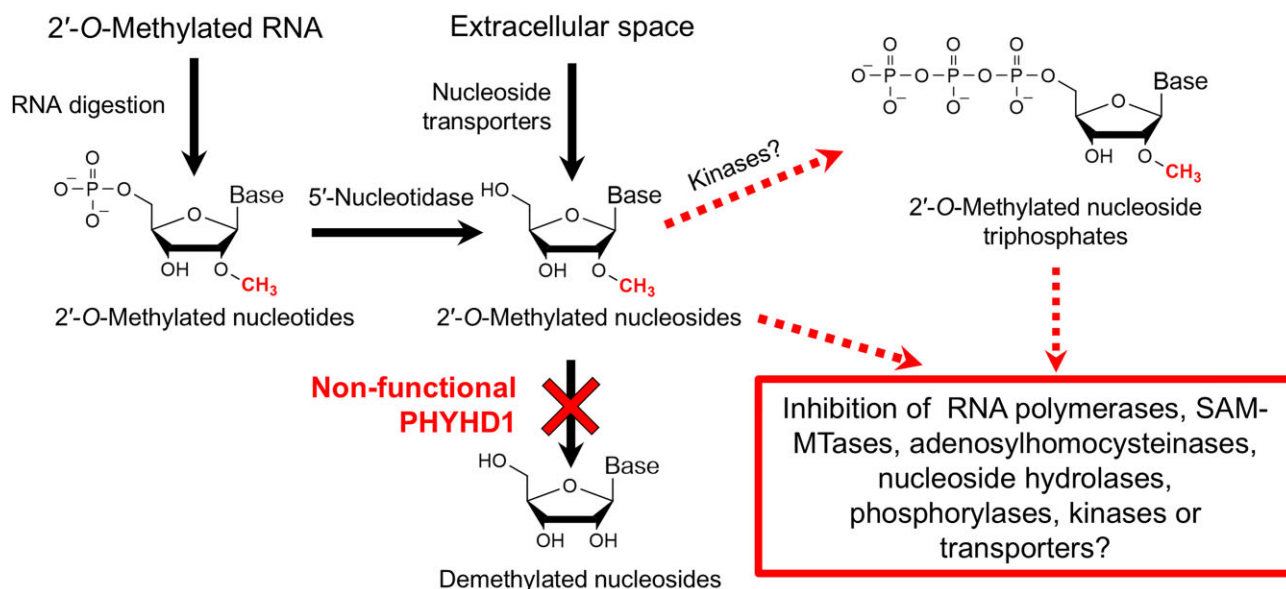


Figure 8. A hypothetical mechanism (indicated by red dotted arrows) by which the lack of functional PHYHD1 might cause negative effects on cellular physiology under abnormal conditions (such as hypoxia). In this model, the accumulation of 2'-O-Me nucleosides leads to the formation of 2'-O-Me nucleoside triphosphates, resulting in the disruption of RNA transcription or metabolic pathways, such as nucleoside salvage.

sulting in elevated levels of free 2'-O-methylated nucleotides, could affect endogenous cellular RNA polymerases and potentially disrupt transcription (Fig. 8). In a less likely scenario, although RNA 2'-O-methylation is typically considered a post-transcriptional modification [2], it is conceivable that under abnormal physiological conditions, elevated levels of 2'-O-methyl nucleoside triphosphates could lead to their incorporation into nascent RNA transcripts by polymerases. This, in turn, may result in unintended 2'-O-methyl modifications within RNA molecules, potentially increasing their resistance to hydrolysis, extending their half-life, and ultimately altering translation dynamics.

Other possible mechanisms include 2'-O-methylated nucleosides acting as active site inhibitors or allosteric regulators of essential enzymes such as S-adenosylmethionine-dependent methyltransferases, S-adenosylhomocysteine hydrolases, nucleoside phosphorylases, kinases, or nucleoside transporters. Thus, an overabundance of these modified nucleosides could disrupt nucleoside salvage pathways, which play a critical role in cellular energy balance and can significantly contribute to glycolysis [74, 75]. Furthermore, given that PHYHD1 is a 2OG oxygenase that requires molecular oxygen for catalysis, it is plausible that hypoxic conditions, such as those found in solid tumours [76], could impact the metabolism of

2'-O-methylated nucleosides. This raises intriguing questions about potential roles of altered modified nucleoside catabolism in the context of pathology.

Taken together, our findings not only shed light on the physiological role of PHYHD1 as a 2'-O-methyl nucleoside demethylase but also illustrate how such insights can emerge from unbiased discovery approaches. Notably, this study began with the functional screening of metagenomic libraries aimed at identifying enzymes involved in the degradation of 2'-O-methylcytidine. This effort led to the discovery of FJS, a previously uncharacterized bacterial dioxygenase, which ultimately guided us toward recognizing a conserved activity in the human homolog, PHYHD1. These results underscore the power of functional screening to uncover novel enzymatic functions that cannot be inferred solely from the sequence data. The ability to identify enzymes whose functions have not been previously described is valuable not only for the search for biocatalysts with environmental, industrial, and biotechnological applications [77] but also for advancing fundamental research [78]. Additionally, functional screening helps to address the limitations of automatic protein function annotation. Many homologous sequences remain misclassified or lack experimentally validated functions, leading to inaccurate predictions of protein activity. Our study serves as a proof-of-concept for the importance of experimental validation, providing insights that may enhance the accuracy of functional annotation and contribute to a broader understanding of the structure–function relationship of enzymes.

Acknowledgements

The authors thank Dr. Justas Vaitekūnas, Dr. Aleksandr Osipenko, and Dr. Janina Ličytė for their technical assistance.

Author contributions: J.S.: Conceptualization, Formal analysis, Investigation, Methodology, Validation, Visualization, Writing – original draft, Writing – review & editing. R.R.: Conceptualization, Investigation, Methodology, Supervision, Validation, Writing – original draft, Writing – review & editing. Ri.M.: Investigation, Methodology. M.J.: Investigation, Methodology, A.A.: Investigation, Methodology, Validation, Writing – review & editing. L.K.: Writing – original draft, Writing – review & editing. J.L.: Investigation, Methodology, Validation. D.B.: Conceptualization, Resources, Writing – review & editing. G.V.: Conceptualization, Resources, Visualization, Writing – review & editing. R.M.: Conceptualization, Funding acquisition, Resources, Supervision, Writing – review & editing.

Supplementary data

Supplementary data is available at NAR online.

Conflict of interest

None declared.

Funding

The Research Council of Lithuania (LMTLT) [S-MIP-24-50 to Ro.M.].

Data availability

All data needed to evaluate the conclusions in the paper are present in the paper and the Supplementary Data. The sequence of metagenome-derived FJS has been uploaded to GenBank (accession code PV755200). The sequences of other recombinant proteins used in this study are available in the Supplementary Data.

References

1. Roundtree IA, Evans ME, Pan T et al. Dynamic RNA modifications in gene expression regulation. *Cell* 2017;169:1187–200. <https://doi.org/10.1016/j.cell.2017.05.045>
2. Zhou KI, Pecot CV, Holley CL. 2'-O-methylation (Nm) in RNA: progress, challenges, and future directions. *RNA* 2024;30:570–82. <https://doi.org/10.1261/rna.079970.124>
3. Dimitrova DG, Teysset L, Carré C. RNA 2'-O-methylation (Nm) modification in human diseases. *Genes* 2019;10:117. <https://doi.org/10.3390/genes10020117>
4. Zhang Y, Lu L, Li X. Detection technologies for RNA modifications. *Exp Mol Med* 2022;54:1601–16. <https://doi.org/10.1038/s12276-022-00821-0>
5. Tang Y, Wu Y, Wang S et al. An integrative platform for detection of RNA 2'-O-methylation reveals its broad distribution on mRNA. *Cell Rep Methods* 2024;4:100721. <https://doi.org/10.1016/j.crmeth.2024.100721>
6. Elliott BA, Ho H-T, Ranganathan SV et al. Modification of messenger RNA by 2'-O-methylation regulates gene expression in vivo. *Nat Commun* 2019;10:3401. <https://doi.org/10.1038/s41467-019-11375-7>
7. Ramachandran S, Krogh N, Jørgensen TE et al. The shift from early to late types of ribosomes in zebrafish development involves changes at a subset of rRNA 2'-O-Me sites. *RNA* 2020;26:1919–34. <https://doi.org/10.1261/rna.076760.120>
8. Hebras J, Krogh N, Marty V et al. Developmental changes of rRNA ribose methylations in the mouse. *RNA Biol* 2020;17:150–64. <https://doi.org/10.1080/15476286.2019.1670598>
9. Maio G, Enweronye O, Zumrut HE et al. Systematic optimization and modification of a DNA aptamer with 2'-O-methyl RNA analogues. *ChemistrySelect* 2017;2:2335–40. <https://doi.org/10.1002/slct.201700359>
10. Ha D-I, Lee JM, Lee N-E et al. Highly efficient and safe genome editing by CRISPR–Cas12a using CRISPR RNA with a ribosyl-2'-O-methylated uridylate-rich 3'-overhang in mouse zygotes. *Exp Mol Med* 2020;52:1823–30. <https://doi.org/10.1038/s12276-020-00521-7>
11. Ke Y, Ghalandari B, Huang S et al. 2'-O-methyl modified guide RNA promotes the single nucleotide polymorphism (SNP) discrimination ability of CRISPR–Cas12a systems. *Chem Sci* 2022;13:2050–61. <https://doi.org/10.1039/D1SC06832F>
12. Sioud M, Furstet G, Cekaitis L. Suppression of immunostimulatory siRNA-driven innate immune activation by 2'-modified RNAs. *Biochem Biophys Res Commun* 2007;361:122–6. <https://doi.org/10.1016/j.bbrc.2007.06.177>
13. Höfler S, Carloniagno T. Structural and functional roles of 2'-O-ribose methylations and their enzymatic machinery across multiple classes of RNAs. *Curr Opin Struct Biol* 2020;65:42–50. <https://doi.org/10.1016/j.sbi.2020.05.008>
14. Ayadi L, Galvanin A, Pichot F et al. RNA ribose methylation (2'-O-methylation): occurrence, biosynthesis and biological functions. *Biochim Biophys Acta* 2019;1862:253–69. <https://doi.org/10.1016/j.bbacta.2018.11.009>
15. Li J, Yang Z, Yu B et al. Methylation protects miRNAs and siRNAs from a 3'-end uridylation activity in *Arabidopsis*. *Curr Biol* 2005;15:1501–7. <https://doi.org/10.1016/j.cub.2005.07.029>

16. Li Y, Yi Y, Gao X *et al.* 2'-O-methylation at internal sites on mRNA promotes mRNA stability. *Mol Cell* 2024;84:2320–36. <https://doi.org/10.1016/j.molcel.2024.04.011>

17. Kawai G, Yamamoto Y, Kamimura T *et al.* Conformational rigidity of specific pyrimidine residues in tRNA arises from posttranscriptional modifications that enhance steric interaction between the base and the 2'-hydroxyl group. *Biochemistry* 1992;31:1040–6. <https://doi.org/10.1021/bi00119a012>

18. Bohnsack MT, Sloan KE. Modifications in small nuclear RNAs and their roles in spliceosome assembly and function. *Biol Chem* 2018;399:1265–76. <https://doi.org/10.1515/hzs-2018-0205>

19. Towns WL, Begley TJ. Transfer RNA methyltransferases and their corresponding modifications in budding yeast and humans: activities, predictions, and potential roles in human health. *DNA Cell Biol* 2012;31:434–54. <https://doi.org/10.1089/dna.2011.1437>

20. Mitsukawa Y, Hibi M, Matsutani N *et al.* A novel nucleoside hydrolase from *Lactobacillus buchneri* LBK78 catalyzing hydrolysis of 2'-O-methylribonucleosides. *Biosci Biotechnol Biochem* 2016;80:1568–76. <https://doi.org/10.1080/09168451.2016.1182853>

21. Mitsukawa Y, Hibi M, Matsutani N *et al.* Enzymatic synthesis of 2'-O-methylribonucleosides with a nucleoside hydrolase family enzyme from *Lactobacillus buchneri* LBK78. *J Biosci Bioeng* 2017;123:659–64. <https://doi.org/10.1016/j.jbiosc.2017.01.005>

22. Mitsukawa Y, Hibi M, Matsutani N *et al.* New nucleoside hydrolase with transribosylation activity from *Agromyces* sp. MM-1 and its application for enzymatic synthesis of 2'-O-methylribonucleosides. *J Biosci Bioeng* 2018;125:38–45. <https://doi.org/10.1016/j.jbiosc.2017.07.016>

23. Aučynaitė A, Rutkienė R, Tauraitė D *et al.* Identification of a 2'-O-methyluridine nucleoside hydrolase using the metagenomic libraries. *Molecules* 2018;23:2904. <https://doi.org/10.3390/molecules23112904>

24. Jia G, Fu Y, Zhao X *et al.* N6-Methyladenosine in nuclear RNA is a major substrate of the obesity-associated FTO. *Nat Chem Biol* 2011;7:885–7. <https://doi.org/10.1038/nchembio.687>

25. Zheng G, Dahl JA, Niu Y *et al.* ALKBH5 is a mammalian RNA demethylase that impacts RNA metabolism and mouse fertility. *Mol Cell* 2013;49:18–29. <https://doi.org/10.1016/j.molcel.2012.10.015>

26. Genz F, Friedrich F, Lönerz C *et al.* Identification and characterization of pyrimidine nucleoside 2'-hydroxylase. *ACS Catal* 2025;15:3611–8. <https://doi.org/10.1021/acscatal.4c07764>

27. Islam MS, Leissing TM, Chowdhury R *et al.* 2-Oxoglutarate-dependent oxygenases. *Annu Rev Biochem* 2018;87:585–620. <https://doi.org/10.1146/annurev-biochem-061516-044724>

28. Martinez S, Hausinger RP. Catalytic mechanisms of Fe(II)- and 2-oxoglutarate-dependent oxygenases. *J Biol Chem* 2015;290:20702–11. <https://doi.org/10.1074/jbc.R115.648691>

29. McDonough MA, Kavanagh KL, Butler D *et al.* Structure of human phytanoyl-CoA 2-hydroxylase identifies molecular mechanisms of Refsum disease. *J Biol Chem* 2005;280:41101–10. <https://doi.org/10.1074/jbc.M507528200>

30. Ala-Nisula T, Sah-Teli SK, Ronkainen V-P *et al.* Human phytanoyl-CoA dioxygenase domain-containing 1 (PHYHD1) is a putative oxygen sensor associated with RNA and carbohydrate metabolism. *FEBS Lett* 2023;597:1651–66. <https://doi.org/10.1002/1873-3468.14666>

31. Zhang Z, Kochan GT, Ng SS *et al.* Crystal structure of PHYHD1A, a 2OG oxygenase related to phytanoyl-CoA hydroxylase. *Biochem Biophys Res Commun* 2011;408:553–8. <https://doi.org/10.1016/j.bbrc.2011.04.059>

32. Zhang H, Huang Z, Song Y *et al.* The TP53-related signature predicts immune cell infiltration, therapeutic response, and prognosis in patients with esophageal carcinoma. *Front Genet* 2021;12:607238. <https://doi.org/10.3389/fgene.2021.607238>

33. Cui J, Wang L, Zhong W *et al.* Identification and validation of methylation-driven genes prognostic signature for recurrence of laryngeal squamous cell carcinoma by integrated bioinformatics analysis. *Cancer Cell Int* 2020;20:472. <https://doi.org/10.1186/s12935-020-01567-3>

34. Cheng S, Xie W, Miao Y *et al.* Identification of key genes in invasive clinically non-functioning pituitary adenoma by integrating analysis of DNA methylation and mRNA expression profiles. *J Transl Med* 2019;17:407. <https://doi.org/10.1186/s12967-019-02148-3>

35. Miyashita A, Hatsuta H, Kikuchi M *et al.* Genes associated with the progression of neurofibrillary tangles in Alzheimer's disease. *Transl Psychiatry* 2014;4:e396. <https://doi.org/10.1038/tp.2014.35>

36. Castillo E, Leon J, Mazzei G *et al.* Comparative profiling of cortical gene expression in Alzheimer's disease patients and mouse models demonstrates a link between amyloidosis and neuroinflammation. *Sci Rep* 2017;7:17762. <https://doi.org/10.1038/s41598-017-17999-3>

37. Yu W, Li Y, Zhong F *et al.* Disease-associated neurotoxic astrocyte markers in Alzheimer disease based on integrative single-nucleus RNA sequencing. *Cell Mol Neurobiol* 2024;44:20. <https://doi.org/10.1007/s10571-024-01453-w>

38. Chen A, Liao P, Li Q *et al.* Phytanoyl-CoA dioxygenase domain-containing protein 1 plays an important role in egg shell formation of silkworm (*Bombyx mori*). *PLoS One* 2021;16:e0261918. <https://doi.org/10.1371/journal.pone.0261918>

39. Naora Y, Hishida Y, Fukazawa T *et al.* Expression analysis of *XPhyH-like* during development and tail regeneration in *Xenopus* tadpoles: possible role of *XPhyH-like* expressing immune cells in impaired tail regenerative ability. *Biochem Biophys Res Commun* 2013;431:152–7. <https://doi.org/10.1016/j.bbrc.2013.01.005>

40. Furusawa Y, Kubo T, Fukazawa T. Phyhd1, an XPhyH-like homologue, is induced in mouse T cells upon T cell stimulation. *Biochem Biophys Res Commun* 2016;472:551–6. <https://doi.org/10.1016/j.bbrc.2016.03.039>

41. Sayers EW, Beck J, Bolton EE *et al.* Database resources of the National Center for Biotechnology Information. *Nucleic Acids Res* 2024;52:D33–43. <https://doi.org/10.1093/nar/gkad1044>

42. Andersen KR, Leksa NC, Schwartz TU. Optimized *E. coli* expression strain LOBSTR eliminates common contaminants from His-tag purification. *Proteins* 2013;81:1857–61. <https://doi.org/10.1002/prot.24364>

43. Aučynaitė A, Rutkienė R, Gasparavičiūtė R *et al.* A gene encoding a DUF523 domain protein is involved in the conversion of 2-thiouracil into uracil. *Environ Microbiol Rep* 2018;10:49–56.

44. Urbelienė N, Kutanovas S, Meškienė R *et al.* Application of the uridine auxotrophic host and synthetic nucleosides for a rapid selection of hydrolases from metagenomic libraries. *Microb Biotechnol* 2018;12:148–60. <https://doi.org/10.1111/1751-7915.13316>

45. Gasteiger E, Hoogland C, Gattiker A *et al.* Protein identification and analysis tools on the ExPASy server. In: Walker JM (ed.), *The Proteomics Protocols Handbook*. Totowa, NJ: Humana Press, 2005, 571–607. <https://doi.org/10.1385/1592598900>

46. Koplūnaitė M, Butkutė K, Špelveris D *et al.* Enzymatic synthesis of modified nucleoside 5'-monophosphates. *Catalysts* 2022;12:1401. <https://doi.org/10.3390/catal12111401>

47. The UniProt Consortium. UniProt: the Universal Protein Knowledgebase in 2025. *Nucleic Acids Res* 2025;53:D609–17. <https://doi.org/10.1093/nar/gkae1010>

48. Katoh K, Rozewicki J, Yamada KD. MAFFT online service: multiple sequence alignment, interactive sequence choice and visualization. *Brief Bioinform* 2019;20:1160–6. <https://doi.org/10.1093/bib/bbx108>

49. Letunic I, Bork P. Interactive Tree of Life (iTOL) v5: an online tool for phylogenetic tree display and annotation. *Nucleic Acids Res* 2021;49:W293–6. <https://doi.org/10.1093/nar/gkab301>

50. Thompson JD, Higgins DG, Gibson TJ. CLUSTAL W: improving the sensitivity of progressive multiple sequence alignment through sequence weighting, position-specific gap penalties and weight

matrix choice. *Nucleic Acids Res* 1994;22:4673–80. <https://doi.org/10.1093/nar/22.22.4673>

51. Tamura K, Stecher G, Kumar S. MEGA11: Molecular Evolutionary Genetics Analysis Version 11. *Mol Biol Evol* 2021;38:3022–7. <https://doi.org/10.1093/molbev/msab120>

52. Jones DT, Taylor WR, Thornton JM. The rapid generation of mutation data matrices from protein sequences. *Comput Appl Biosci* 1992;8:275–82. <https://doi.org/10.1093/bioinformatics/8.3.275>

53. Felsenstein J. Confidence limits on phylogenies: an approach using the bootstrap. *Evolution* 1985;39:783–91. <https://doi.org/10.1111/j.1558-5646.1985.tb00420.x>

54. Abramson J, Adler J, Dunger J et al. Accurate structure prediction of biomolecular interactions with AlphaFold 3. *Nature* 2024;630:493–500. <https://doi.org/10.1038/s41586-024-07487-w>

55. Röhrig UF, Goullioux M, Bugnon M et al. Attracting Cavities 2.0: improving the flexibility and robustness for small-molecule docking. *J Chem Inf Model* 2023;63:3925–40. <https://doi.org/10.1021/acs.jcim.3c00054>

56. Bugnon M, Röhrig UF, Goullioux M et al. SwissDock 2024: major enhancements for small-molecule docking with attracting cavities and AutoDock Vina. *Nucleic Acids Res* 2024;52:W324–32. <https://doi.org/10.1093/nar/gkae300>

57. Meng EC, Goddard TD, Pettersen EF et al. UCSF ChimeraX: tools for structure building and analysis. *Protein Sci* 2023;32:e4792. <https://doi.org/10.1002/pro.4792>

58. Guerra JV, da S, Ribeiro-Filho HV et al. pyKVFinder: an efficient and integrable Python package for biomolecular cavity detection and characterization in data science. *BMC Bioinformatics* 2021;22:607. <https://doi.org/10.1186/s12859-021-04519-4>

59. Yang Z, Vilkaitis G, Yu B et al. Approaches for studying microRNA and small interfering RNA methylation *in vitro* and *in vivo*. *Methods Enzymol* 2007;427:139–54. [https://doi.org/10.1016/S0076-6879\(07\)27008-9](https://doi.org/10.1016/S0076-6879(07)27008-9)

60. Jao L-E, Wente SR, Chen W. Efficient multiplex biallelic zebrafish genome editing using a CRISPR nuclease system. *Proc Natl Acad Sci USA* 2013;110:13904–9. <https://doi.org/10.1073/pnas.1308335110>

61. Stanislauskienė R, Laurynėnas A, Rutkienė R et al. YqfB protein from *Escherichia coli*: an atypical amidohydrolase active towards N4-acylcytosine derivatives. *Sci Rep* 2020;10:788. <https://doi.org/10.1038/s41598-020-57664-w>

62. Aučynaitė A, Rutkienė R, Tauraitė D et al. Identification of a 2'-O-methyluridine nucleoside hydrolase using the metagenomic libraries. *Molecules* 2018;23:E2904. <https://doi.org/10.3390/molecules23112904>

63. Kazlauskas A, Darinskas A, Meškys R et al. Isocytosine deaminase Vcz as a novel tool for the prodrug cancer therapy. *BMC Cancer* 2019;19:197. <https://doi.org/10.1186/s12885-019-5409-7>

64. Sayers EW, Beck J, Bolton EE et al. Database resources of the National Center for Biotechnology Information in 2025. *Nucleic Acids Res* 2025;53:D20–9. <https://doi.org/10.1093/nar/gkae979>

65. Camacho C, Coulouris G, Avagyan V et al. BLAST+: architecture and applications. *BMC Bioinformatics* 2009;10:421. <https://doi.org/10.1186/1471-2105-10-421>

66. Saari RE, Hausinger RP. Ascorbic acid-dependent turnover and reactivation of 2,4-dichlorophenoxyacetic acid/alpha-ketoglutarate dioxygenase using thiophenoxyacetic acid. *Biochemistry* 1998;37:3035–42. <https://doi.org/10.1021/bi97238p>

67. Mantri M, Zhang Z, McDonough MA et al. Autocatalysed oxidative modifications to 2-oxoglutarate dependent oxygenases. *FEBS J* 2012;279:1563–75. <https://doi.org/10.1111/j.1742-4658.2012.08496.x>

68. Andreani J, Schulz F, Di Pinto F et al. Morphological and genomic features of the new *Klosneuvirinae* isolate fadolivirus IHUMI-VV54. *Front Microbiol* 2021;12:719703. <https://doi.org/10.3389/fmicb.2021.719703>

69. Vilkaitis G, Plotnikova A, Klimasauskas S. Kinetic and functional analysis of the small RNA methyltransferase HEN1: the catalytic domain is essential for preferential modification of duplex RNA. *RNA* 2010;16:1935–42. <https://doi.org/10.1261/rna.2281410>

70. Liew WC, Orbán L. Zebrafish sex: a complicated affair. *Brief Funct Genomics* 2014;13:172–87. <https://doi.org/10.1093/bfgp/elt041>

71. Darst BF, Lu Q, Johnson SC et al. Integrated analysis of genomics, longitudinal metabolomics, and Alzheimer's risk factors among 1,111 cohort participants. *Genet Epidemiol* 2019;43:657–74. <https://doi.org/10.1002/gepi.22211>

72. Cerezo M, Sollis E, Ji Y et al. The NHGRI-EBI GWAS Catalog: standards for reusability, sustainability and diversity. *Nucleic Acids Res* 2025;53:D998–1005. <https://doi.org/10.1093/nar/gkae1070>

73. Carroll SS, Tomassini JE, Bosserman M et al. Inhibition of hepatitis C virus RNA replication by 2'-modified nucleoside analogs. *J Biol Chem* 2003;278:11979–84. <https://doi.org/10.1074/jbc.M210914200>

74. Giannecchini M, Matteucci M, Pesi R et al. Uptake and utilization of nucleosides for energy repletion. *Int J Biochem Cell Biol* 2005;37:797–808. <https://doi.org/10.1016/j.biocel.2004.10.005>

75. Skinner OS, Blanco-Fernández J, Goodman RP et al. Salvage of ribose from uridine or RNA supports glycolysis in nutrient-limited conditions. *Nat Metab* 2023;5:765–76. <https://doi.org/10.1038/s42255-023-00774-2>

76. Liao C, Liu X, Zhang C et al. Tumor hypoxia: from basic knowledge to therapeutic implications. *Semin Cancer Biol* 2023;88:172–86. <https://doi.org/10.1016/j.semcancer.2022.12.011>

77. Thapa S, Li H, OHair J et al. Biochemical characteristics of microbial enzymes and their significance from industrial perspectives. *Mol Biotechnol* 2019;61:579–601. <https://doi.org/10.1007/s12033-019-00187-1>

78. Ufarté L, Potocki-Veronese G, Laville É. Discovery of new protein families and functions: new challenges in functional metagenomics for biotechnologies and microbial ecology. *Front Microbiol* 2015;6:563. <https://doi.org/10.3389/fmicb.2015.00563>